

### 5.1 Synthesis of Polymer Conjugates

The polymers used were polyethylenimine 2 kDa (PEI2), polyethylenimine 25 kDa (PEI25) and polyallylamine 15 kDa (PAA15). The synthesis of polymer conjugates of polyethylenimine and polyallylamine with cholic acid (ChA) was carried out in order to alter the lipophilicity of these polymers so that the resulting polymer conjugates with different hydrophobicities can be used as gene carriers. One of the reasons for selecting cholic acid was the fact that it is biosynthesized in the body and it is a biocompatible material. Another reason for its selection being its unique structural feature of having three hydroxyl groups placed axially on one side. Such a structural arrangement represents a planar amphiphile as opposed to head-to-tail amphiphiles (Walker S. *et al.* 1996) and it has a steroid backbone in its structure. It is reported that steroid receptors are present on nuclear membrane (Rebuffat et al-2001) and recently it was shown that bile acids are natural ligands to farnesoid x receptor(FXR) (Hua T. et al-2000). Moreover, the bile acids and their derivatives are known to interact and destabilize the membranes (cell and endosomal membrane) owing to their amphiphilic characters. Hence, it was envisioned in the present work that by substituting the polymers (PEI2, PEI25 and PAA15), the transfection efficiency could be increased while minimizing their toxicity. The conjugates were synthesized by coupling primary amine (-NH<sub>2</sub>) group of polymers with the carboxyl (-COOH) group of ChA using carbodiimide chemistry (see schemes below). The solvent selection is an integral part of any reaction because the judicious choice of solvent can afford ready separation of unreacted reactants, by-products and the resultant desired product.

An exhaustive physical solubility study was carried out for the polymers and cholic acid and the solvents were selected on the basis of solubility differences of the polymers and cholic acid. The reaction of PEI2 and PEI25 polymers were carried out in CHCl<sub>3</sub> with DCC as coupling agent and the reaction of PAA was carried out in 1:1 water:methanol mixture with EDC as coupling agent. The high quality (as confirmed by clean NMR spectra for products) PEI conjugates was obtained by purifying the reaction products with ether precipitation method. For PAA conjugates, a white precipitate was obtained that weighed more than the total weight of cholic acid and unmodified polymer weight added to the reaction. Thus, it was concluded that the product (i.e. PAA15-ChA conjugate) was containing

large amount of byproduct (i.e. impurities). Hence, the PAA conjugates were purified using dialysis method.

The reaction of carbodiimide is simple one step one pot reaction, but the reaction involves a complicated mechanism that has been explained by Nakajima and Ikada (Nakajima N. and Ikada Y. 1995). Carbodiimide chemistry has been widely used in the field of bioconjugation (Hoffmann C. *et al.* 2011), peptide synthesis (Wang D. *et al.* 1987) and modifications of polysaccharides (Darr A. and Calabro A. 2009). The carbodiimide-mediated amide bond formation is a simple reaction that uses non-hazardous reagents and can be carried out in an aqueous solution and at room temperature. Additionally, this reaction is most likely to preserve the molecular distribution of complex molecules. 1-ethyl-3-(3-dimethylaminopropyl) carbodiimide (EDC) is the most commonly used carbodiimide because of its aqueous solubility, whereas N, N'-dicyclohexylcarbodiimide (DCC) is employed where reaction is carried out in organic solvents. The toxicity of the carbodiimide reaction has been estimated to be low since EDC/DCC is transformed into a non-toxic urea derivative in the coupling reaction (Hermanson G.T.-2008).

The schematic of amide bond formation using carbodiimide chemistry has been shown in figure 5.1. The carbodiimide reacts with carboxylic groups of fatty acid, the reaction between a carboxyl group and carbodiimide results in a urea on which a primary amine (nucleophile) can attack, resulting in an amide bond formation. The coupling is a zero-length crosslinker, meaning no additional residues besides the amide bond have been added to cholic acid

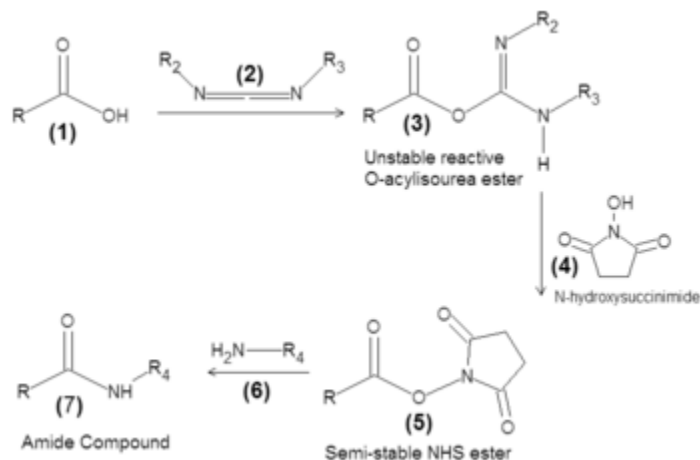


Figure 5.1: Schematic of amide bond formation using carbodiimide chemistry

The amide bond formation using carbodiimide chemistry has been explained in detail (Hermanson G.T.-2008). The carbodiimide-mediated coupling of a fatty acid (1) with a primary amine compound (6) using EDC/DCC first progressed through an unstable intermediate, an O-acylisourea ester compound (3) formed by the reaction of the carbodiimide (2) with the fatty acid. Because this intermediate is unstable (i.e. short lived), NHS (N-hydroxysuccinimide) was added to the cholic acid together with the carbodiimide to form an NHS-ester (5), which was a more reactive with amines. Upon the final addition of a primary amine containing polymer (6) the desired polymer conjugate with an amide bond (7) was formed by displacement of the NHS.

The reaction product was purified either by ether precipitation method (in case of PEI conjugates) or dialysis method (for PAA conjugates) by low MWCO dialysis tubes. The carbodiimide-mediated coupling of a cholic acid with primary amines of polyethylenimine (figure 5.2) and polyallylamine (figure 5.3) is shown as below:

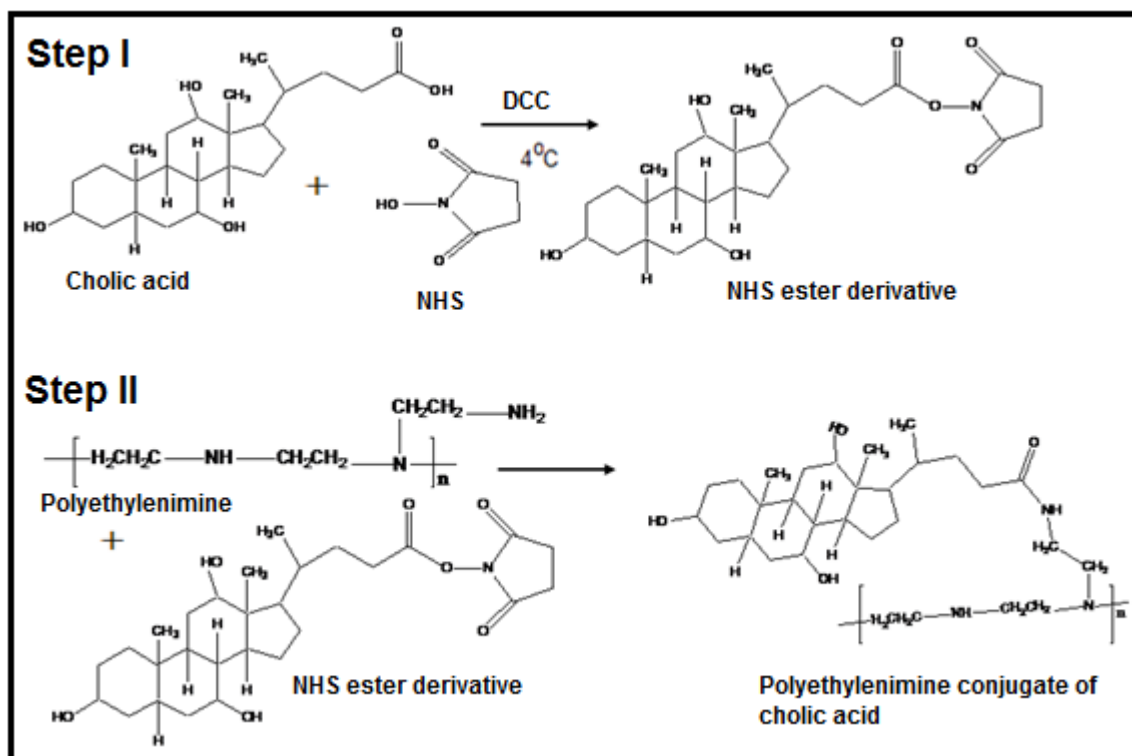


Figure 5.2: Schematic of cholic acid polymer conjugate (PEI-ChA) formation using polyethylenimine and cholic acid.

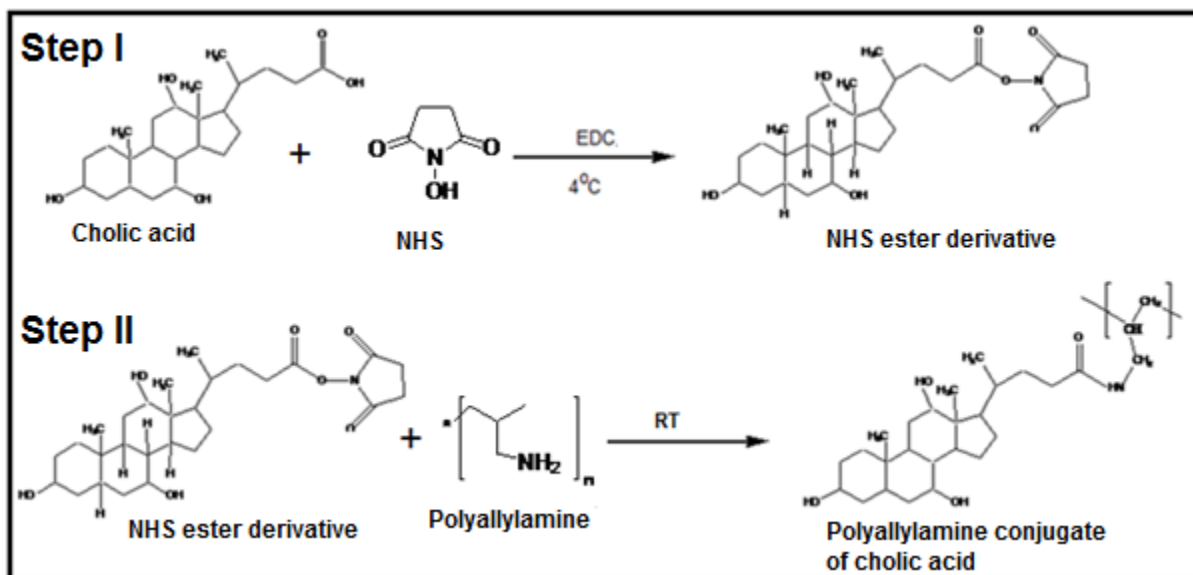


Figure 5.3: Schematic of synthesis of cholic acid polymer conjugates with polyethylenimine/polyallylamine (PEI/PAA)

## 5.2 Characterization of Polymer Conjugates

### 5.2.1 Structural Analysis by $^1\text{H-NMR}$

Synthesized polymer conjugates and plain polymers were characterized and confirmed by  $^1\text{H-NMR}$  spectra (Bruker 300 MHz). The unique and characteristics peak of polymers (PEI2, PEI25 and PAA15) and cholic acid were identified for calculating substitution level achieved. Specific peaks were confirmed by unmodified samples of PEI, PAA and ChA prior to conjugate analysis. The degree of substitution was determined by characteristic peak integrations corresponding to PEI ( $-\text{NH}-\underline{\text{C}}\text{H}_2-\underline{\text{C}}\text{H}_2-\text{NH}-$ ;  $\delta \sim 2.5-3.0$  ppm) and PAA ( $\text{NH}_2-\underline{\text{C}}\text{H}_2-\text{CH}$ ;  $\sim \delta 1.3-1.7$  ppm) with respect to terminal methyl group of the ChA ( $-\underline{\text{C}}\text{H}_3$ ;  $\delta \sim 0.95$  ppm). Figure 5.4 and 5.5 shows typical  $^1\text{H-NMR}$  of ChA in  $\text{D}_2\text{O}$  with characteristic peaks corresponding to ChA protons, typical  $^1\text{H-NMR}$  of ChA substituted PEI2 in DMSO with characteristic peaks corresponding to PEI ( $\delta \sim 2.5-2.8$  ppm) and ChA protons ( $\delta \sim 0.95$  ppm), respectively. Figure 5.6 shows typical  $^1\text{H-NMR}$  of ChA substituted PAA15 in DMSO with characteristic peaks corresponding to PAA15 ( $\delta \sim 1.3-1.7$  ppm) and ChA protons ( $\delta \sim 0.95$  ppm). The NMR spectra for PEI2, PAA15 and their conjugates are shown in figure 5.7 and 5.8.

The formula used for calculation of substitution level achieved for polymer conjugates based on NMR spectra is shown in equation 5.1 and 5.2. The DP in the equation stands for degree of polymerization which was calculated theoretically based on molecular weight and number of repeating units.

$$\text{Substitution ratio} = \frac{\frac{\text{\# protons for lipid (practical)}}{\text{\# protons for lipid (theoretical)}}}{\frac{\text{\# protons for polymer (practical)}}{\text{\# protons for polymer (theoretical)}}} * DP \dots\dots\dots \text{Equation 5.1}$$

$$\text{Substitution ratio} = \frac{\frac{\text{\# x (corres.to 3 H atoms from CH}_3 \text{ at } \delta^- 0.8)}{\text{3 (theoretical)}}}{\frac{\text{\# y (corres.to 4 H atoms from two CH}_2 \text{ units at } \delta^- 2.5-2.8)}{\text{4 (theoretical)}}} * DP \dots\dots\dots \text{Equation 5.2}$$

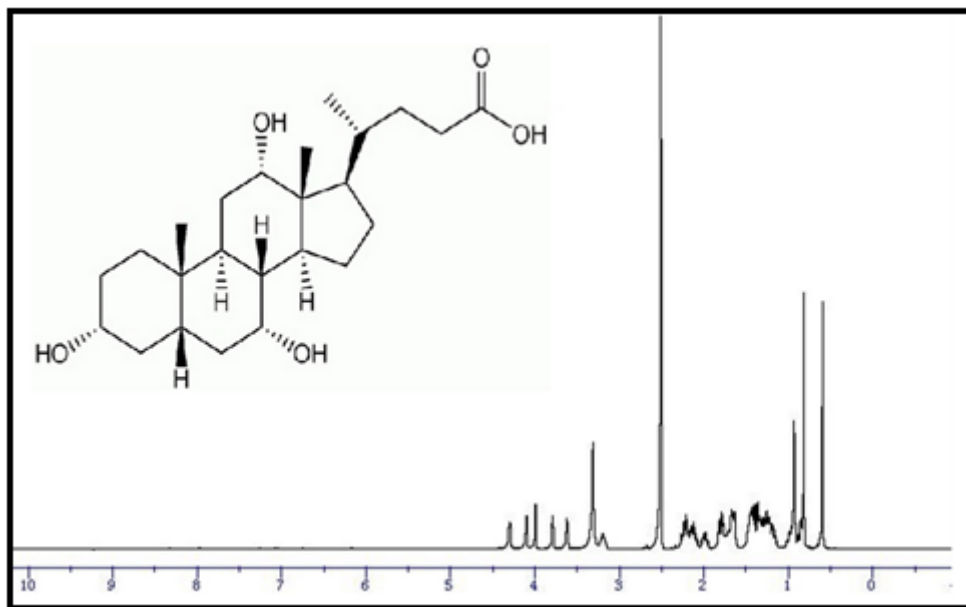


Figure 5.4: Typical  $^1\text{H-NMR}$  of ChA in  $\text{D}_2\text{O}$  showing characteristic peaks corresponding to ChA protons ( $\delta \sim 0.95$  ppm).

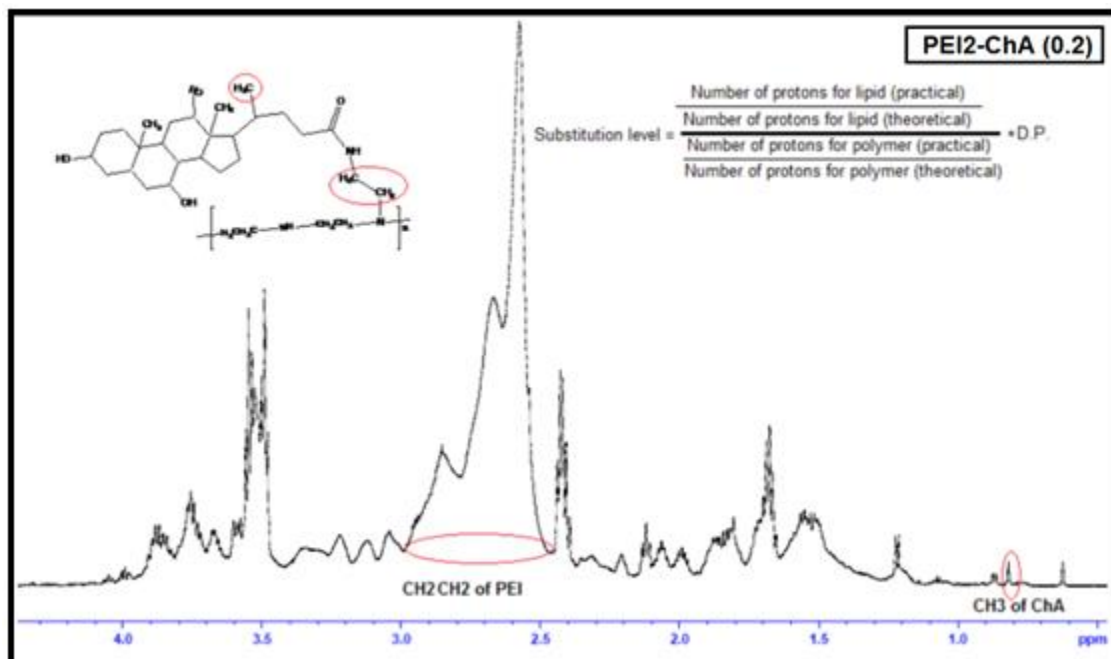


Figure 5.5: Typical  $^1\text{H-NMR}$  of ChA substituted PEI2 in DMSO, showing characteristic peaks corresponding to PEI ( $\delta \sim 2.5\text{-}2.8$  ppm) and ChA protons ( $\delta \sim 0.95$  ppm).

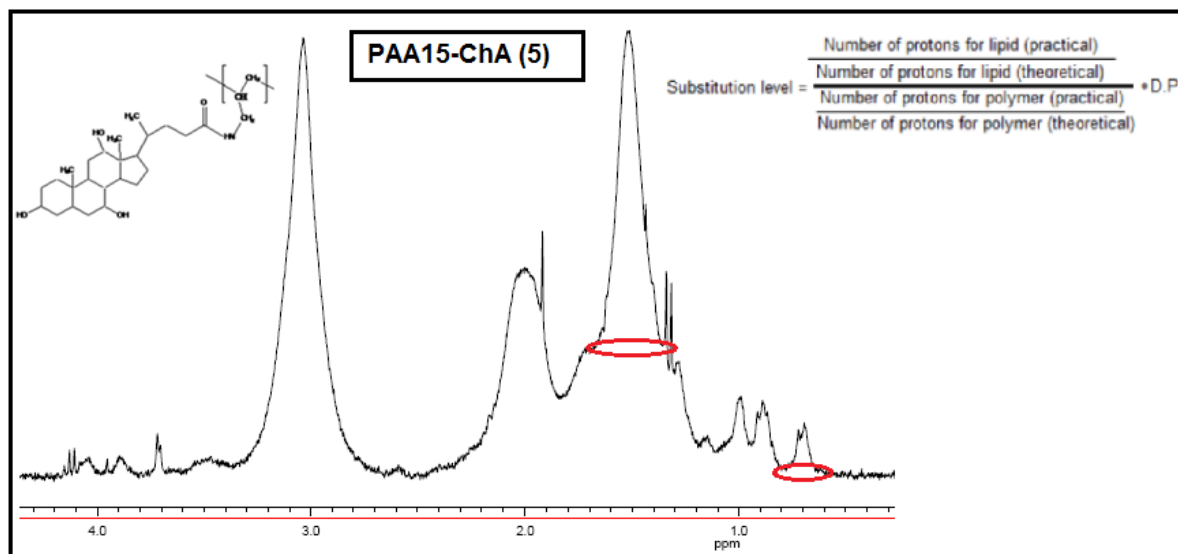


Figure 5.6: Typical  $^1\text{H-NMR}$  of ChA substituted PAA15 in D<sub>2</sub>O, showing characteristic peaks corresponding to PAA ( $\delta \sim 1.3\text{-}1.7$  ppm) and ChA protons ( $\delta \sim 0.95$  ppm).

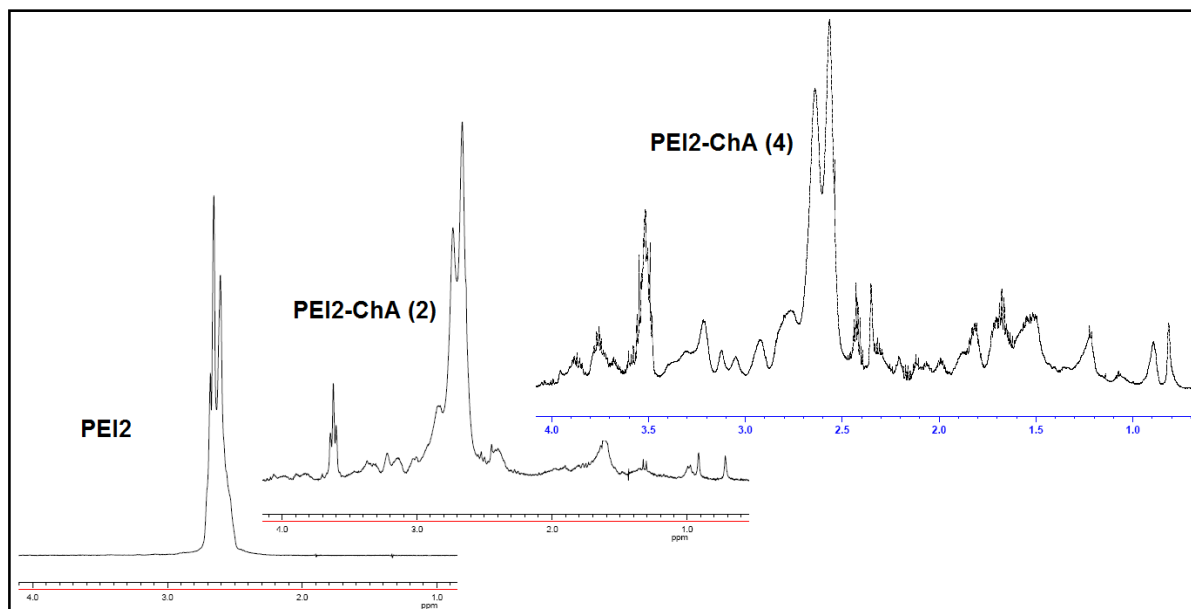


Figure 5.7:  $^1\text{H-NMR}$  spectra PEI2 and ChA substituted PEI2 in DMSO, showing characteristic peaks corresponding to PEI ( $\delta\sim 2.5\text{-}2.8$  ppm) and ChA protons ( $\delta\sim 0.95$  ppm).

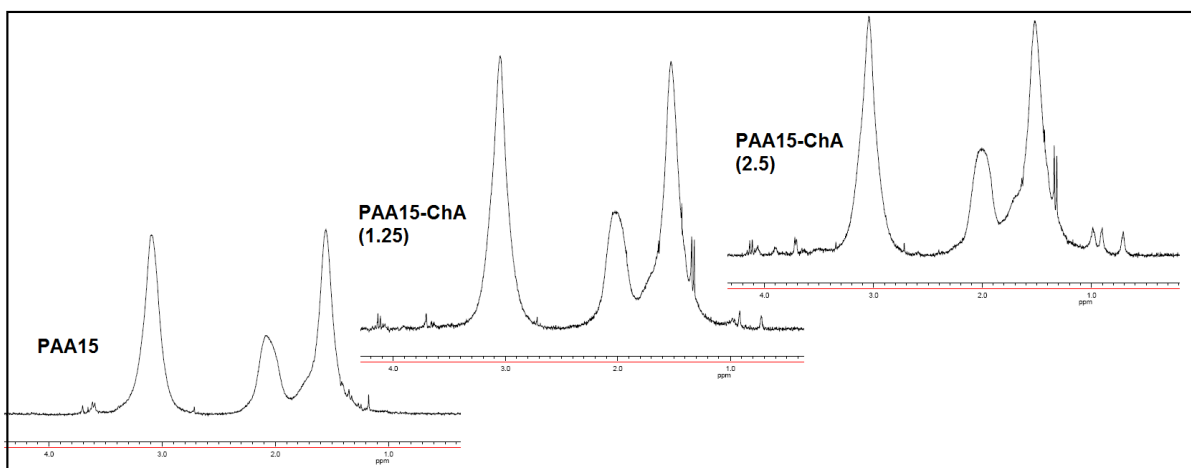


Figure 5.8:  $^1\text{H-NMR}$  spectra PAA15 and ChA substituted PAA15 in D<sub>2</sub>O, showing characteristic peaks corresponding to PAA ( $\delta\sim 1.3\text{-}1.7$  ppm) and ChA protons ( $\delta\sim 0.95$  ppm).

The correlation between the lipid:polymer feed ratio (mol/mol) and the substitution level of cholic acid achieved per polymer unit of all three polymers is shown in table 5.1. A clear correlation was obtained between lipid:polymer molar feed ratio and the substitution level achieved for all three polymers (Figure 5.10). A generally linear dependence of final ChA substitution ratio on the initial feed ratio was seen in figure 5.9. The number of lipids

substituted per PEI increased with increased molecular weight of the polymer (PEI2 to PEI25). For a polymer (PEI2):lipid feed ratio of 0.2 to 4, number of lipids per PEI was increased from 0.53 to 1.90, whereas for PEI25 4.9 to 14.3 lipid per PEI25 were obtained when feed ratio (polymer:lipid) 0.2 to 16 was used. The lipid substitution for PAA15 was also increased from 0.89 to 6.7 for lipid:PAA15 feed ratio of 1.25 to 10. All the polymer conjugates were found to be soluble in water, except the highest substituted PEI25-ChA which was not used for further studies.

Table 5.1: Substitution level achieved for polymer conjugates corresponding to theoretical feed ratio of lipid:polymer (mol/mol).

S. No.	Polymer Conjugate	Feed ratio (lipid: polymer), mol/mol	Substitution Level (ChA per polymer unit) Achieved
1.	PEI2-ChA (0.2)	0.2	0.53
2.	PEI2-ChA (0.5)	0.5	0.43
3.	PEI2-ChA (1)	1	0.60
4.	PEI2-ChA (2)	2	1.59
5.	PEI2-ChA (4)	4	1.90
6.	PEI2-ChA (5)	5	2.20
7.	PEI25-ChA (0.2)	0.2	4.94
8.	PEI25-ChA (2)	2	5.03
9.	PEI25-ChA (4)	4	5.99
10.	PEI25-ChA (16)	16	14.31
11.	PAA15-ChA (1.25)	1.25	0.89
12.	PAA15-ChA (2.5)	2.5	2.29
13.	PAA15-ChA (5)	5	3.23
14.	PAA15-ChA (10)	10	6.70

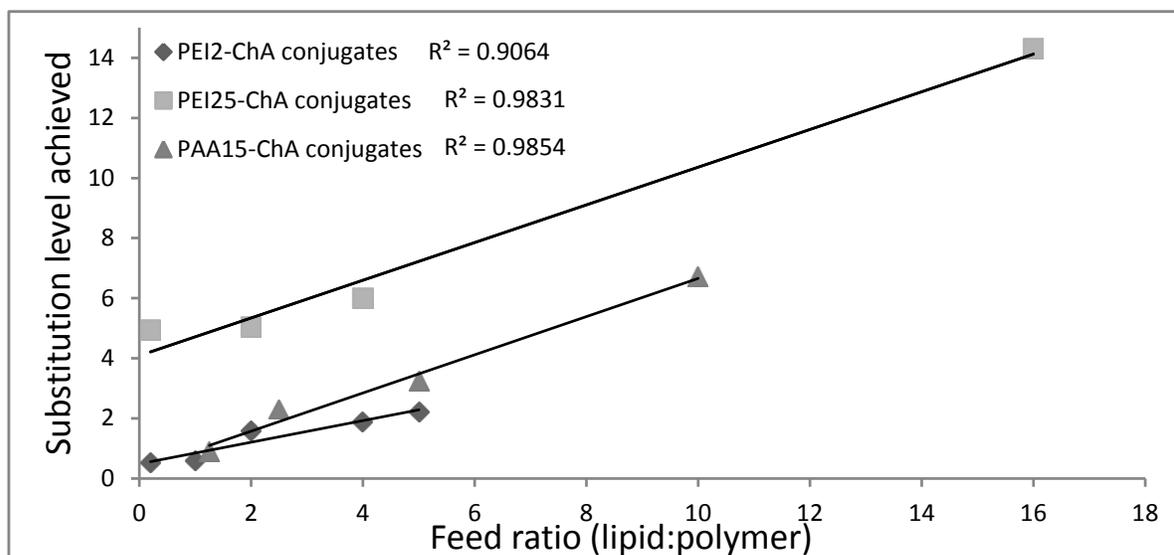


Figure 5.9: Correlation between the lipid:polymer feed ratio (mol:mol) and the substitution levels achieved for PEI2-ChA, PEI25-ChA and PAA15-ChA conjugates.

### 5.2.2 SYBR Green I Binding Assay

All the studies upto cell cycle analysis were carried out using plasmid gWIZ-GFP (reporter plasmid) encoding for green fluorescent protein (GFP).

The ability of polymer conjugates and unmodified polymers (PEI2, PEI25 and PAA15) to bind the plasmid DNA was calculated by SYBR Green I assay and the concentration for effective condensation of the pDNA (i.e., polymer/pDNA weight ratio required to complex 50% of pDNA, BC50) were calculated. The binding curves as a function of polymer/pDNA weight ratios were plotted for all three series of cholic acid conjugates in figure 5.10. It should be noted that values in triplicate were used for analysis by SigmaPlot 11.0 software. The pDNA binding capacity of polymer conjugates for PEI25 (figure 5.10B) and PAA15 (figure 5.10C) remained relatively unaltered while the binding capacity of PEI2 (figure 5.10A) conjugates were found to be significantly decreased with increasing substitution. This decreased binding capacity of PEI2 conjugates as compared to that of unmodified PEI2 can be attributed to significant consumption of relatively low content of primary amines, which are responsible for pDNA condensation (Bahadur K. C. *et al*-2011).

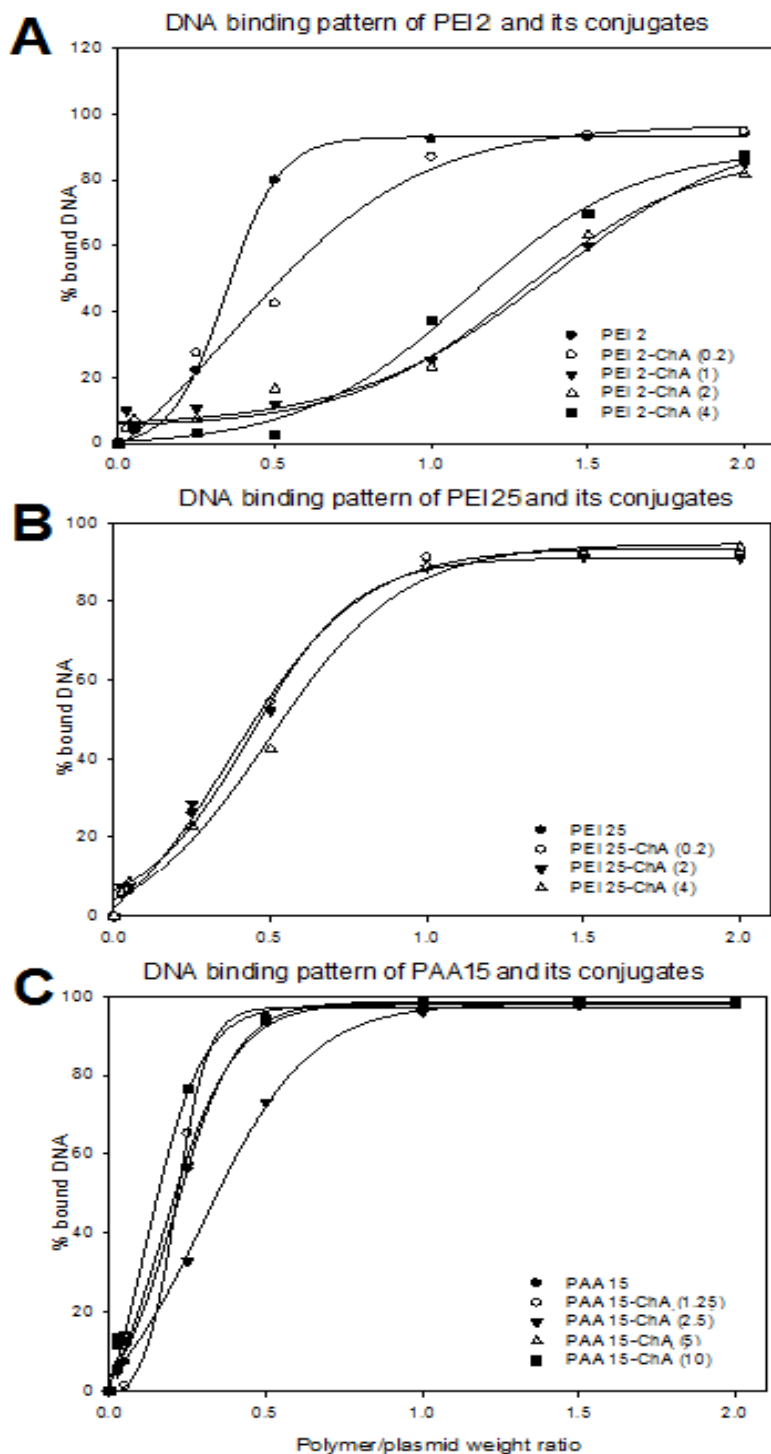


Figure 5.10: Binding curves for three series of polymer conjugates (A. PEI2, B. PEI25, and C. PAA15) as obtained after complexation with pDNA at different polymer:plasmid weight ratios. %pDNA binding values obtained from SYBR green I assay were plotted against polymer:plasmid weight ratios.

The weaker binding of PEI2-ChA conjugates could be indicated by the increased fluorescence intensity that could occur only when the SYBR Green I dye had an access to the pDNA. Therefore, continued access of SYBR Green I dye to loosely-bound pDNA might explain relatively weaker binding of the PEI2 conjugates. Table 5. 2, 5. 3 and 5. 4 show the average % bound pDNA values for unmodified polymer and its conjugates (PEI2, PEI25 and PAA15) corresponding to different polymer to plasmid DNA weight ratio.

Table 5.2: Average % bound pDNA values for unmodified polymer and its conjugates (PEI2) corresponding to different polymer to plasmid DNA weight ratio.

Polymer:pDNA weight ratio	AVG of % bound pDNA				
	PEI2	PEI2-ChA (0.2)	PEI2-ChA (1)	PEI2-ChA (2)	PEI2-ChA (4)
0	0	0	0	0	0
0.025	0.6884	2.9172	9.9523	4.7518	0.0592
0.05	4.0385	4.0575	6.3395	7.2218	4.5918
0.25	22.1355	27.2990	10.6112	7.3042	3.2387
0.5	79.8593	42.3515	11.7701	16.3726	2.4623
1	92.1294	86.8636	25.1193	23.0769	37.2079
1.5	92.8377	93.7095	59.9205	63.2957	69.7782
2	93.9850	94.5965	84.9262	81.6043	87.4002

Table 5.3: Average % bound pDNA values for unmodified polymers and their conjugates (PEI25) corresponding to different polymer to plasmid DNA weight ratio.

Polymer:pDNA weight ratio	AVG of % bound pDNA			
	PEI25	PEI25-ChA (0.2)	PEI25-ChA (2)	PEI25-ChA (4)
0	0	0	0	0
0.025	5.4121	5.4121	7.2984	5.6840
0.05	6.4453	6.4453	7.9445	8.6946
0.25	26.1943	22.6199	28.5858	22.5674
0.5	54.2460	54.2460	52.1273	42.4807
1	91.1218	91.1218	88.5463	88.8536
1.5	92.1419	92.1419	91.1366	92.5354
2	92.4686	92.4686	90.9452	93.6751

Table 5.4: Average % bound pDNA values for unmodified polymers and their conjugates (PAA15) corresponding to different polymer to plasmid DNA weight ratio.

Polymer:pDNA weight ratio	AVG of % bound pDNA				
	PEI2	PEI2-ChA (0.2)	PEI2-ChA (1)	PEI2-ChA (2)	PEI2-ChA (4)
0	0	0	0	0	0
0.025	13.5177	2.0260	4.7531	6.5197	11.7232
0.05	7.3733	1.2662	14.1214	13.3677	12.4608
0.25	56.3011	65.2707	32.8427	58.2020	76.4234
0.5	93.8756	94.4255	73.1570	94.6936	94.0552
1	98.2551	97.5896	95.9469	97.4185	98.3923
1.5	98.5174	98.6360	97.9580	97.9522	98.3719
2	98.5846	97.9316	98.4630	97.9922	98.3001

### 5.2.3 Electrophoretic Mobility Shift Assay (EMSA)

The polymer conjugates and unmodified polymers (PEI2, PEI25 and PAA15) have ability to bind to the plasmid DNA and this was qualitatively analyzed (visualized) by EMSA

assay (figure 5.11, 5.12 and 5.13). As shown in figure 5.12 and 5.13 the pDNA binding capacity of polymer conjugates for PEI25 and PAA15 remained relatively unaltered while the binding capacity of PEI2 (Figure 5.11) conjugates were found to be significantly decreased with increasing substitution. These results are in accordance with the SYBR Green I assay where decreased binding capacity of PEI2 conjugates was attributed to significant consumption of relatively low content of primary amines, which are responsible for pDNA condensation, by lipid substitution (Bahadur K. C. et al-2011). Alternatively, continued access of SYBR Green I dye to loosely-bound pDNA might explain relatively weaker binding of the PEI2 conjugates. The binding capacity of highest substituted PEI2 conjugate (PEI2-ChA(4)) was significantly lower as compared to that of unmodified PEI2 (figure 5.11).

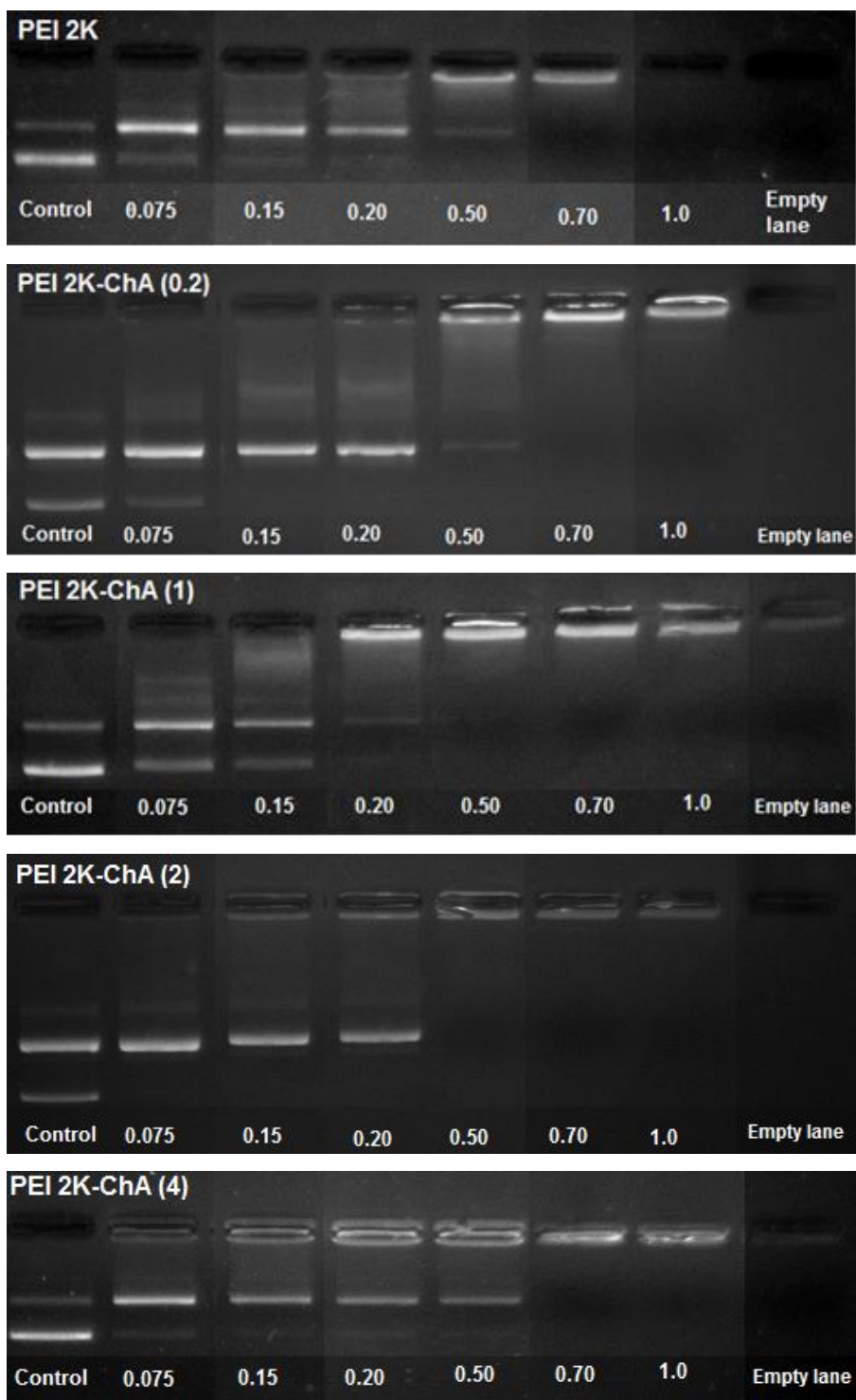


Figure 5.11: EMSA for PEI2 and PEI2-ChA conjugates.

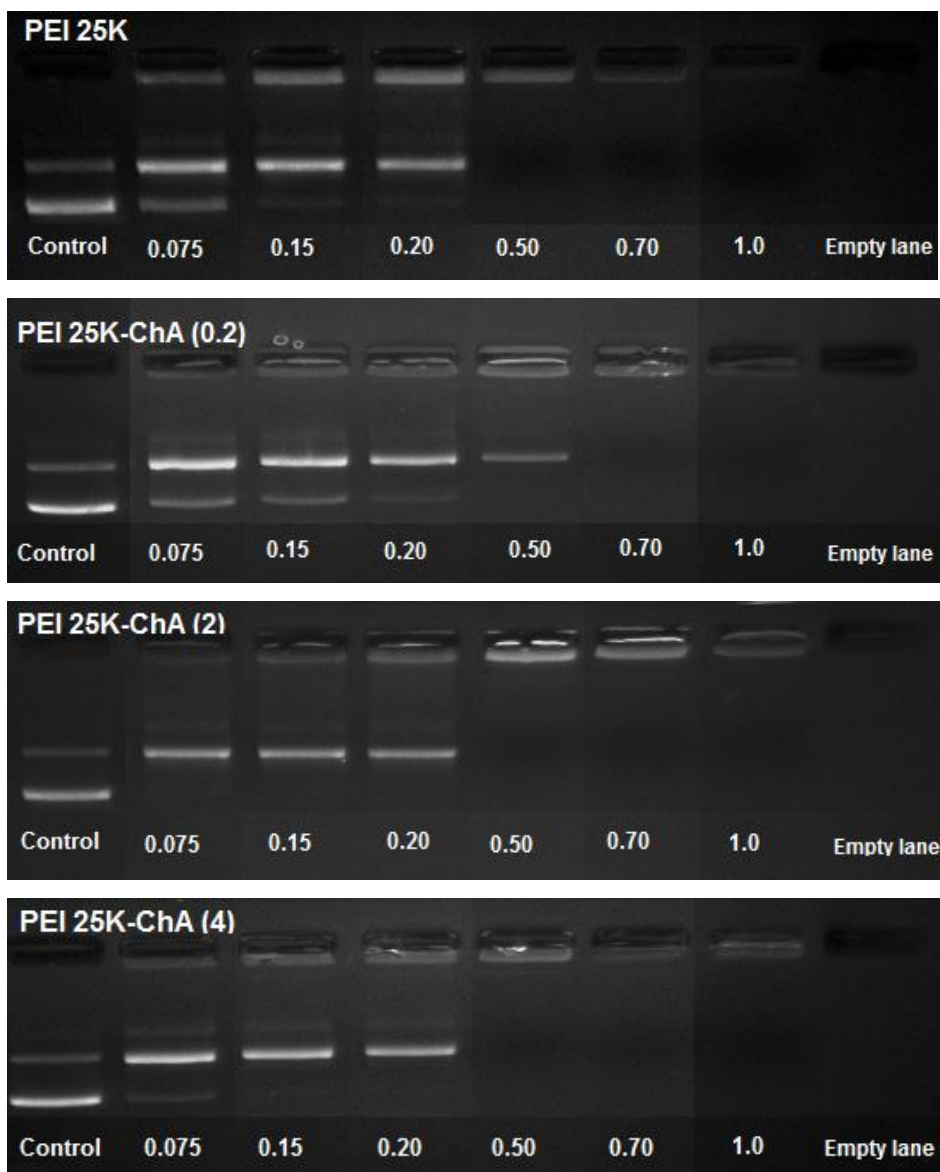


Figure 5.12: EMSA for PEI25 and PEI25-ChA conjugates.



Figure 5.13: EMSA for PAA15 and PAA15-ChA conjugates.

A graph was plotted for polymer:pDNA weight ratio against 100% binding as observed visually in EMSA and BC50 values obtained from SYBR green I assay (figure 5.14). It seems that PEI2 conjugates showed a trend of increased BC50 values as a function of lipid substitution, whereas both PEI25 and PAA15 conjugates showed no clear trend between two

parameters. There was no clear trend could be observed from 100% binding as observed visually in EMSA.

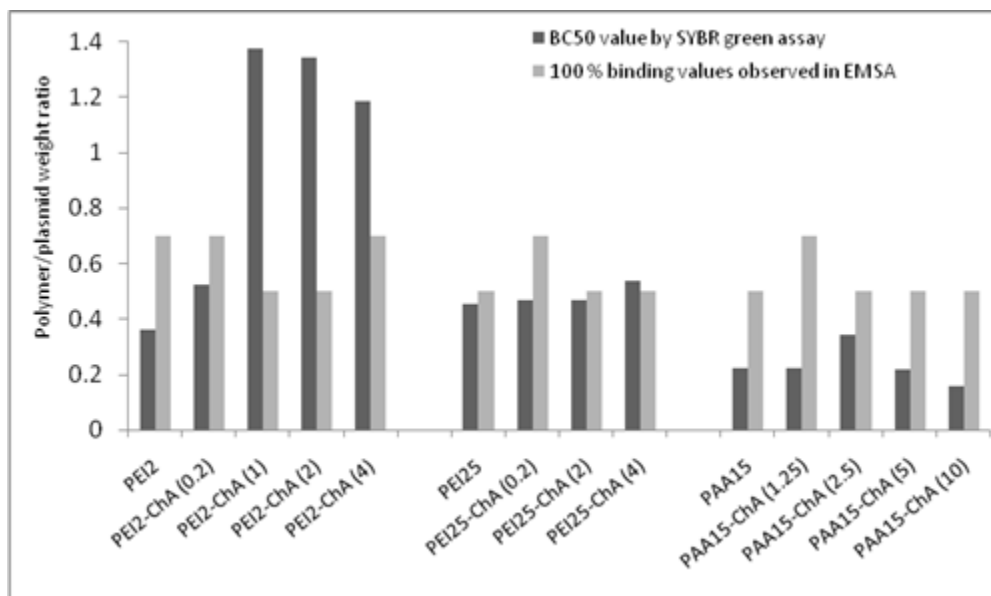


Figure 5.14: Comparison of BC50 values and 100% binding values as obtained by SYBR green I assay and EMSA, respectively, for three different polymers and their conjugates at various polymer:plasmid DNA weight ratios.

#### 5.2.4 DNase I Protection Assay

The plasmid DNA complexes with cationic carriers exposed to cleavage by DNase I should be carried out to test the ability of these complexes in protecting DNA from digestion by DNase present in serum (Al-Deena F.N. et al-2013). Polyplexes should be able to protect DNA from extracellular and intracellular DNase and this ability to protect the plasmid DNA was evaluated by a study of DNA protection against DNase I. It is highly desirable for the plasmid DNA complexes with cationic carriers (polymer/lipid) to protect the pDNA against DNase I for at least 1 h (Du Y. et al-2011). As shown in the figure 5.15, the intensity of pDNA bands indicated that all polymer conjugates at polymer:plasmid DNA weight ratio of 5 and above, protected at least ~50% of pDNA amount up to 1 h treatment with DNase I at the ratio used for transfection studies (i.e. polymer:plasmid DNA weight ratio of 10). Moreover, no smear of pDNA was seen in the gel electrophoresis which implies that the pDNA was intact during the test period. It implies that the nanoplexes prepared with polymer

conjugates (PEI2, PEI25 and PAA15) could be used in vivo owing to their ability to protect pDNA against DNase which is present in extra and intracellularly.

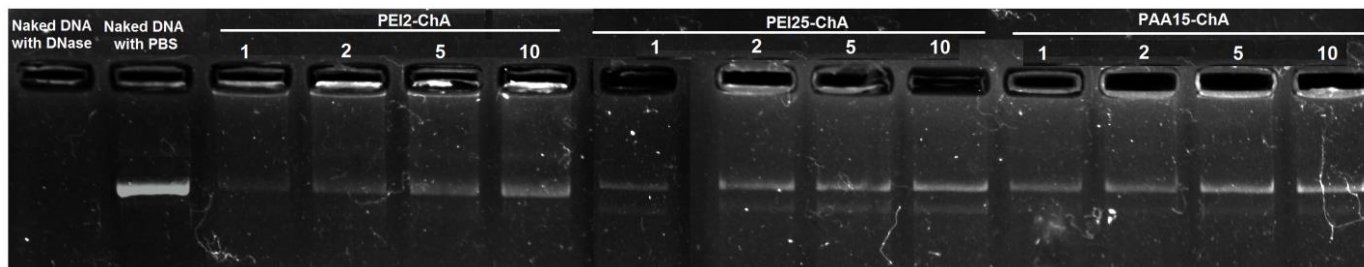


Figure 5.15: Protection of plasmid DNA by polymer and polymer conjugates against DNase I treatment.

### 5.2.5 Heparin Challenge/Dissociation Assay

Nanoplexes are expected to demonstrate stability in the presence of anionic serum proteins encountered in vivo. In addition, after cellular uptake of polyplexes, dissociation of polyplexes is also necessary for effective translation of transgene towards synthesis of encoded proteins. To better investigate dissociation, a well-established anion challenge assay was carried out using heparin to evaluate extent of pDNA dissociation from the polyplexes (Moret I. et. al-2001).

The qualitative evaluation of dissociation of complexes by anion (heparin) challenge at various concentrations (0.01, 0.05, 0.1, 0.5 mg/ml) was monitored as shown in figure 5.16 & 5.17. As observed in figure 5.17, it was found that unmodified PEI2, PEI25 and PAA15 were so tightly bound to plasmid DNA that dissociation of complexes was observed only with 1 mg/ml heparin solution. Polymer conjugates of PEI25 and PAA15 were slightly less tightly bound to plasmid DNA (0.5 mg/ml heparin required for complete dissociation), whereas PEI2-ChA was less tightly bound to pDNA requiring 0.1 mg/ml heparin concentration for complete dissociation. The weak binding strength of PEI2-ChA was attributed to relatively less number of primary amines available for binding to pDNA after modification by cholic acid (explained by SYBR Green I and EMSA assay).

The nanoplexes of both PEI2 and PEI2-ChA, prepared in presence of serum (5% FBS) were more stable and resisted dissociation by heparin as compared to the nanoplexes prepared without serum (figure 5.17). It can be explained by the fact that serum contains

anionic proteins and hence the complexes prepared in presence of anions are strong enough to resist dissociation of complexes at higher concentrations of heparin. It should be noted that complexes of PEI2 prepared in serum free saline solution dissociated at 0.25 mg/ml heparin concentration (figure 5.16) whereas, the complexes of PEI2 prepared in serum containing saline dissociated at 0.5 mg/ml heparin concentration (figure 5.17). Similarly, the complexes of PEI2-ChA prepared in serum free saline solution dissociated at 0.05 mg/ml heparin concentration (figure 5.16) whereas, the complexes of PEI2 prepared in serum containing saline dissociated at 0.1 mg/ml heparin concentration (figure 5.18).

Based on the results of DNase protection (figure 5.15) and dissociation assay (figure 16 and 5.17), it implies that yet polymer conjugates of PEI2 bind to pDNA less tightly but the binding is sufficient to protect the pDNA against degradation by DNase I. Further, it means that the nanoplexes prepared with conjugates of PEI2 would protect pDNA extracellularly and would release it intracellularly (owing to less tight binding) after their uptake, thereby improving transfection efficiency.

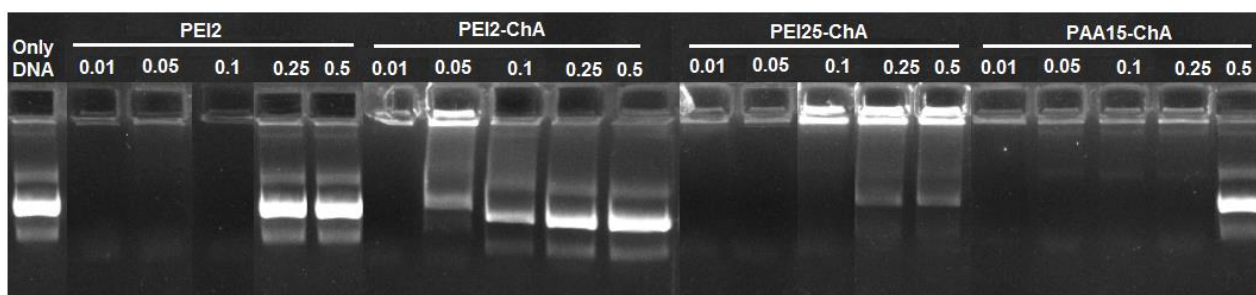


Figure 5.16: Qualitative evaluation of dissociation of nanoplexes of polymer conjugates with pDNA by anion (heparin) challenge at concentrations 0.01, 0.05, 0.1, 0.5 mg/ml (the complexes were formed in 150 mM saline).

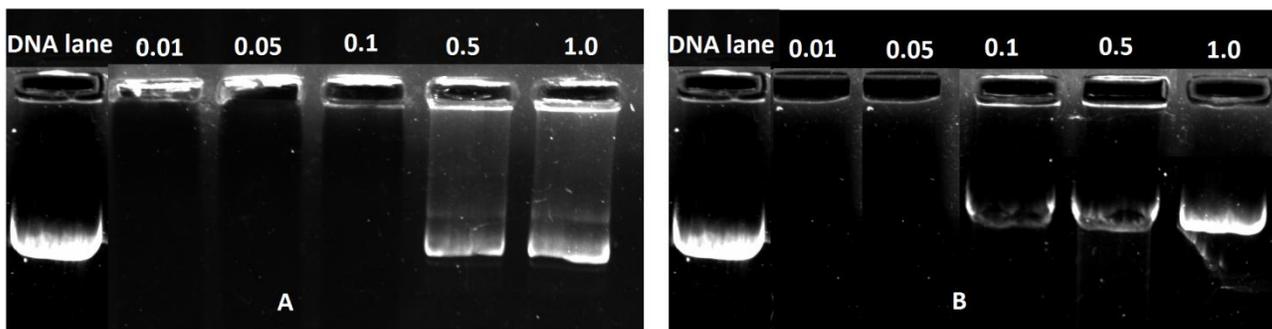


Figure 5.17: Dissociation assay for nanoplexes by anion challenge (heparin), at concentrations ranging from 0.01 mg/ml to 1.0 mg/ml (the complexes were formed in 150 mM saline with 10% DMEM containing 5% serum) **A.** assay results for PEI2 and **B.** assay results for PEI2-ChA nanoplexes.

### 5.2.6 Cytotoxicity Assay by MTT

The cytotoxicity of the chosen polymers and their ChA conjugates is summarized in figure 5.18. PEI2 polymer did not show cytotoxicity on the 293T cells (figure 5.18A), consistent with the known compatibility of this polymer with the mammalian cells (Shen Y.-2013). As ChA is biocompatible lipid, its conjugation with PEI2 also did not indicate an increase its cytotoxicity. Hydrophobic modifications of PEI2 with lipid (palmitic acid, myristic acid and linoleic acid) were previously shown to increase their cytotoxicity on several cell types, for example in 293T cells with lipid palmitic acid (Bahadur K. C. *et al*-2011) and in BMSC cells with myristic and stearic acid (Neamark A. *et al*-2009). The use of natural compounds in the preparation of new materials can improve the biocompatibility of the materials and avoid any potential toxicity of the degradation products when used for biomedical applications. Moreover, the polymers made of biosynthesized and biocompatible materials can be promising in both biomedical and pharmaceutical fields. The fact that no incremental toxicity was observed for polymer conjugates as compared to their unmodified counterparts (figure 5.18), it implies that the ChA as a lipid substituent might be more compatible than the aliphatic lipids previously used (Neamark A. *et al*-2009 and Bahadur K. C. *et al*-2011). Bile acids are amphiphilic molecules biosynthesized in the liver (Zhang J.W. and Zhu X.X.-2009) and this explains no apparent increase in cytotoxicity of the polymer.

The polymer conjugates of PEI2 (polymer conjugates with lower substitution levels) gave apparent viabilities ~100% and this was attributed to activation of cellular metabolic pathways (i.e., succinate dehydrogenase in the TCA cycle, the enzyme responsible for MTT conversion) without significant damage to cellular metabolism (Neamnark A. et al-2009).

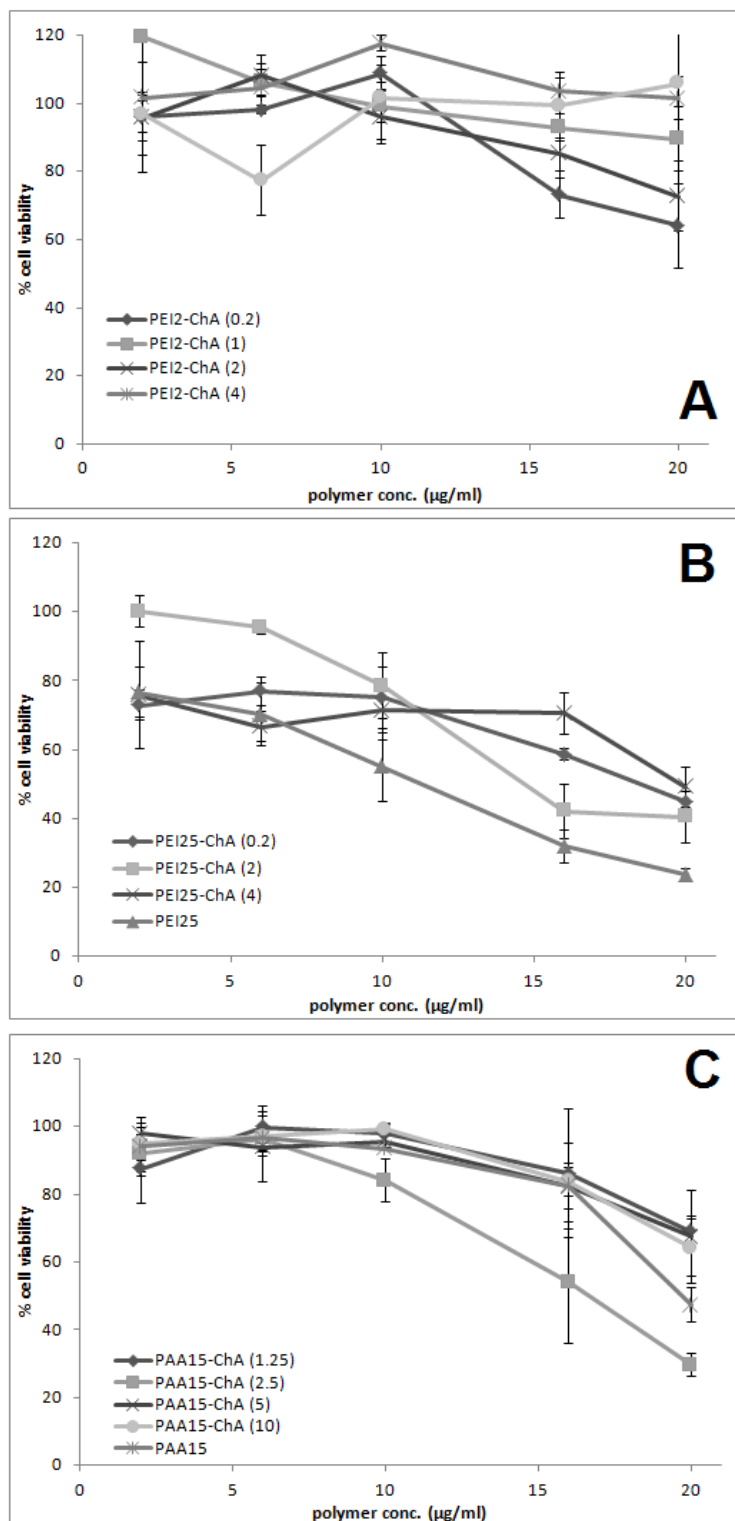


Figure 5.18: The cytotoxicity of PEI2 (Panel A), PEI25 (Panel B) and PAA15 (Panel C) polymers and their ChA conjugates on 293T cells.

The cytotoxicity of PEI25 was evident in the clear dose-response curve seen in figure 5.18B, and ChA modification of PEI25, in general, decreased the cytotoxicity of PEI25. The consumption of some of the primary amines) was likely the reason for the decreased cytotoxicity. The PAA15 similarly displayed a dose-dependent cytotoxicity (figure 5.18C), albeit to a lower extent than the PEI25 owing to high amount of primary amines that interact with cell membranes. In this case, ChA conjugation to PAA15 increased the cytotoxicity which might be possible as a result of imparting enhanced interaction with the cell membrane due to the ChA. Thus, it implies that ChA substitution is safe in case of both the PEI used in the present work (PEI2 and PEI25) and warrants their *in vitro* and *in vivo* applications.

### 5.3 Formulation of nanoplexes

The nanoplexes were prepared by ionic complexation between polymer conjugates and plasmid DNA achieved by electrostatic interactions between the negatively charged phosphate groups of DNA and the positively charged amine groups of polymer conjugates. The molecular weight, chain length and structure (branched vs linear) of a polymer have a significant effect on its size and zeta potential (Ko Y. T. et al 2011). Moreover, the polymer to plasmid weight ratio also does have directly proportional effect on size of the nanoplexes formed.

It was previously reported that folate-linked cationic nanoparticles could deliver DNA with high transfection efficiency *in vitro* when the nanoparticle/plasmid DNA complex (nanoplex) was formed in 150 mM NaCl solution (Hattori Y. et al-2005). Hence, we prepared the nanoplexes in 150 mM saline solution. The nanoplexes were then prepared with transferrin as a ligand (Ogris M. et al-1998) that may serve two purposes, firstly, it is used as a brain targeting ligand and secondly it can be used as a shielding agent (Kircheis R. et al-2001). The nanoplexes of unmodified polymers and polymer conjugates prepared at different polymer to plasmid weight ratio yielded small (table 5.5) round shaped compact nanoparticles as shown in TEM images (figure 5.23).

## 5.4 Characterization of Nanoplexes

### 5.4.1 Dynamic Light Scattering (DLS) Studies

The particle sizes of nanoplexes prepared with polymer or polymer conjugates with plasmid DNA were recorded (Brookhaven 90Plus, USA). The dynamic light scattering analysis showed that the hydrodynamic diameter of various nanoplexes (with three different polymer conjugate series) measured was within the range of 100-230 nm (table 5.5). The particle size distribution pattern indicated that all particles are of nanometer size with polydispersity index of less than 0.45 and devoid of any aggregates.

Table 5.5: Particle size of the nanoplexes prepared with different polymers or polymer conjugates (three different series) prepared in 150 mM saline at polymer:plasmid ratio of 10.

S. No.	Sample name	Mean particle size (nm)	SD ( $\pm$ )
1	PEI2	139.7	10.85
2	PEI2 –ChA (0.2)	174.8	15.10
3	PEI2 –ChA (1)	133.6	12.34
4	PEI2 –ChA (2)	109.6	9.90
5	PEI2 –ChA (4)	101.1	11.52
6	PEI25	141.7	8.36
7	PEI25 –ChA (0.2)	122.5	5.47
8	PEI25 –ChA (2)	113.3	17.21
9	PEI25–ChA (4)	99.8	22.31
10	PAA15	155.6	14.66
11	PAA15–ChA (1.25)	159.3	9.70
12	PAA15–ChA (2.5)	155.7	15.57
13	PAA15–ChA (5)	156.5	20.33
14	PAA15–ChA (10)	142.0	20.62
15	PEI2 with Tf	226.3	11.50
16	PEI2 –ChA (4) with Tf	185.9	10.82

It can be easily seen from the figure 5.19 that in case of the PEI2 and PEI25 polymers, the particle sizes of modified polymers i.e. polymer conjugates were smaller as compared to their native counterparts, with the exception of PEI-ChA (0.2) which showed increased particle size. In case of PAA15 conjugate series, the particle size remained unchanged. A similar observation was also reported by Zheng et al. that lipoic acid conjugation to PEI-1.8 via dicyclo hexylcarbodiimide (DCC)/N-hydroxysuccinimide (NHS) coupling also reduced particle size (Zheng M. *et al*-2012). The polymer conjugates of PEI2 and PEI25 (substitution ratio: 4) were able to condense plasmid DNA to form complexes with smaller sizes (90 nm to 100 nm) and this was attributed to increased hydrophobic interactions which have been shown to aid in particle assembly (Grzelczak M. *et al*-2010). The PEI2-ChA conjugates only were studied for transferrin incorporation. The incorporation of transferrin to the nanoplexes system of polymer or polymer conjugate with pDNA showed an increase in particle size ~80 nm which was attributed to bulky nature of the ligand. Figure 5.20 shows the typical particle size distribution graph showing hydrodynamic diameter for nanoplexes prepared.

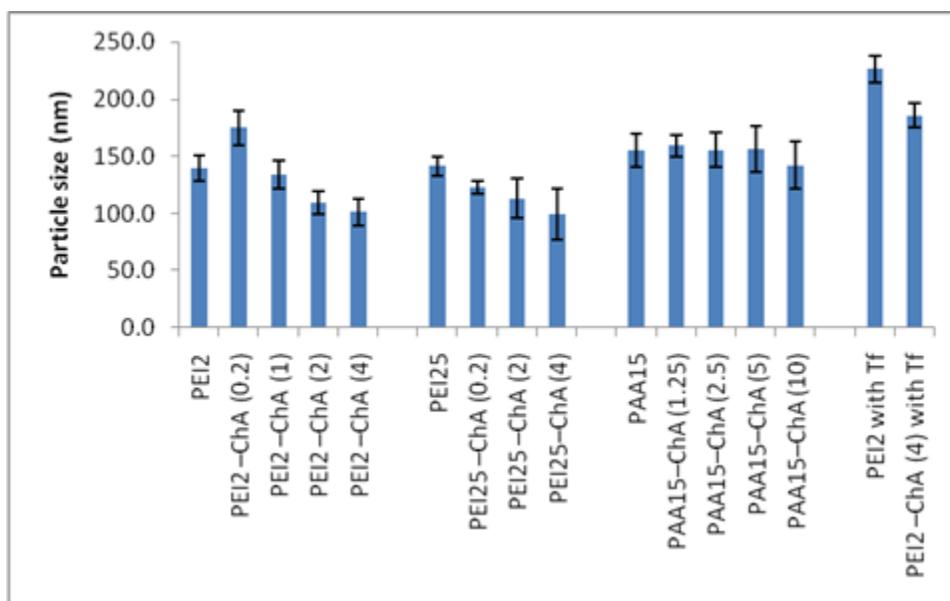


Figure 5.19: Particle size of the nanoplexes prepared with different polymers (PEI2, PEI25 and PAA15) or their conjugates.

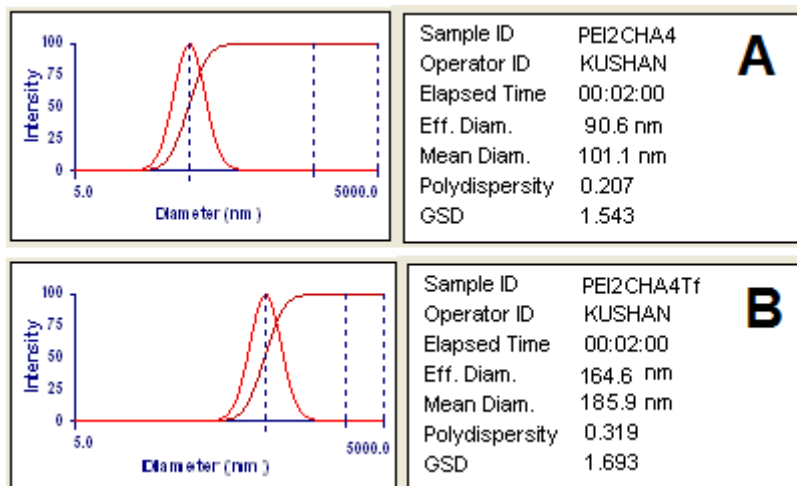


Figure 5.20: Typical particle size distribution graph showing hydrodynamic diameter (in nm).

#### 5.4.2 Zeta Potential Studies

In addition to small size, a cationic surface charge is also desired as it helps in electrostatic interaction between nanoplexes and anionic proteoglycans, such as syndecan, on cell surfaces, resulting in increased endocytosis (Gratton S.A. *et al*-2008, Kopatz I. *et al*-2004). The zeta potential ( $\zeta$ ) pattern indicated that all particles have positive zeta potential with smaller standard deviation, which means that the nanoplexes would help in binding to cell surface (Table 5.6).

Table 5.6: Zeta potential ( $\zeta$ ) of the nanoplexes prepared with different polymers or polymer conjugates.

S. No.	Sample name	Mean Zeta potential (mV)	SD ( $\pm$ )
1	PEI2	16.61	4.71
2	PEI2 –ChA (0.2)	16.75	4.29
3	PEI2 –ChA (1)	17.00	2.65
4	PEI2 –ChA (2)	26.51	5.37
5	PEI2 –ChA (4)	27.71	7.09
6	PEI25	17.59	4.63
7	PEI25 –ChA (0.2)	18.00	4.33
8	PEI25 –ChA (2)	25.64	3.52
9	PEI25–ChA (4)	28.18	5.17
10	PAA15	17.67	3.77
11	PAA15–ChA (1.25)	18.50	3.94
12	PAA15–ChA (2.5)	18.88	2.84
13	PAA15–ChA (5)	24.76	5.42
14	PAA15–ChA (10)	25.51	4.73
15	PEI2 with Tf	3.90	1.28
16	PEI2 –ChA (4) with Tf	5.62	2.00

The zeta potential of transferrin containing nanoplexes was also positive. But the overall positive charge for transferrin containing nanoplexes is decreased significantly owing to its negative charge. The reduction in resulting surface charge may reduce the nonspecific interaction with anionic proteins that occurs in blood circulation *in vivo* and may act as shield against opsonization. Moreover, transferrin may enhance uptake of nanoplexes in the brain cells by transferrin receptor (TfR) mediated endocytosis (Ogris M. et al-1998). The zeta potential measurements showed that nanoplexes formed by PEI2-ChA and PEI25-ChA at higher substitution levels had higher cationic charge (~25-30 mV) than unmodified PEI2 and PEI25 (~17 mV) (figure 5.21). A similar phenomenon was also reported in DNA complexes

formed with lipid-modified low molecular weight PEI (Zheng M. *et al*-2002 and Bahadur K.R. *et al*-2011). Figure 5.22 shows the typical zeta potential ( $\zeta$ ) graph showing zeta potential ( $\zeta$ ) in mV for nanoplexes (with and without Tf) prepared in 150 mM saline at polymer to plasmid ratio of 10. This higher ( $\sim 10$ ) overall positive of nanoplexes imparts stability in solution (Neu M. *et al*-2006) and may help them avoid charge-charge interaction among each other.

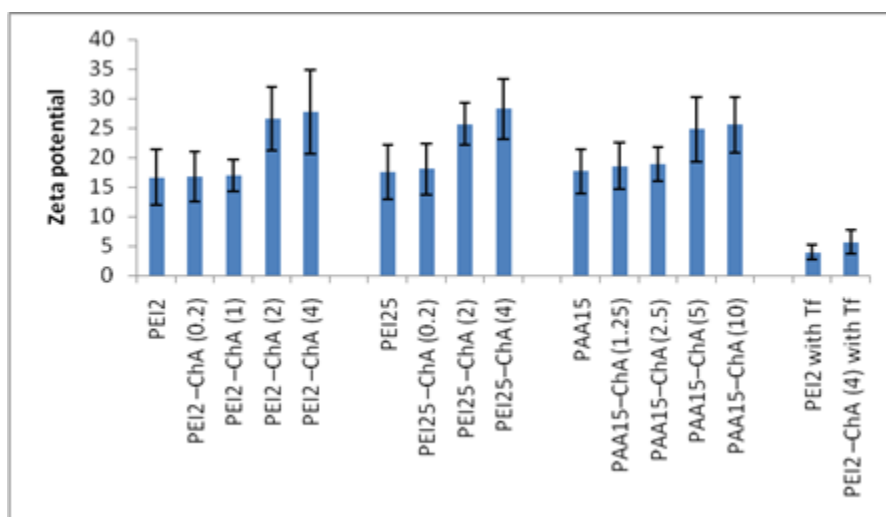


Figure 5.21: Zeta potential ( $\zeta$ ) of nanoplexes prepared with different polymers (PEI2, PEI25 and PAA15) or their conjugates.

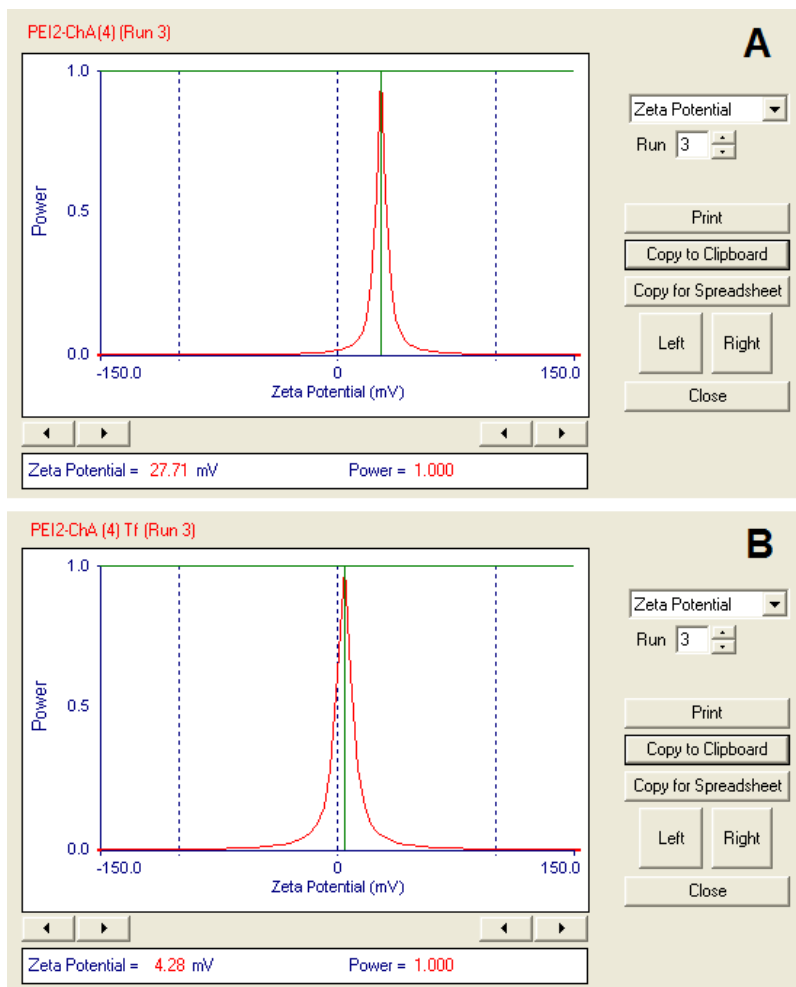


Figure 5.22: Typical zeta potential ( $\zeta$ ) graph showing zeta potential ( $\zeta$ ) in mV for nanoplexes with Tf (A) and without Tf (B).

### 5.4.3 Transmission Electron Microscopy

The transmission electron microscopy (TEM) images were recorded to find out the structure and morphology of nanoplexes, also it serves as a direct measure of particle size (Philips/FEI (Morgagni)). The sample preparation was carried out in ultrapure water so as to avoid precipitates of salt that would have formed on the grid. The TEM images revealed that particles (nanoplexes) formed by polymer conjugates with pDNA were compact, solid and spherical in shape (fig 5.23). Also it was observed that polymer conjugates formed smaller sized particles with plasmid DNA as compared to their unmodified counterparts.

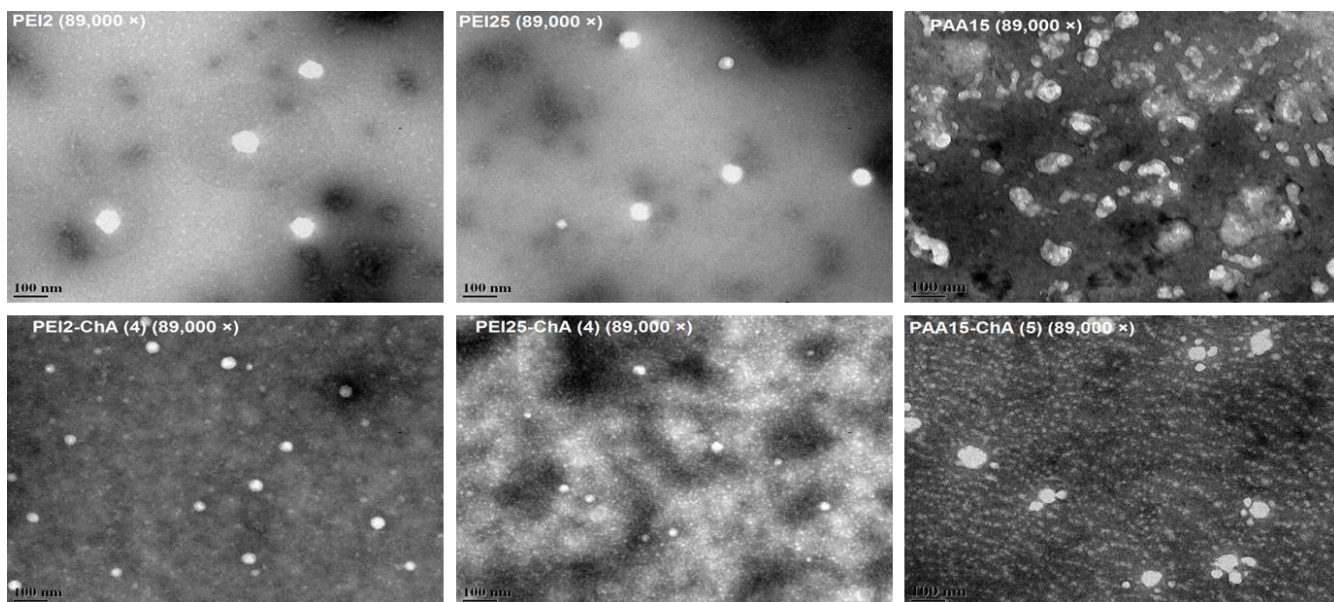


Figure 5.23: Morphology of nanoplexes (89,000 $\times$  magnification) made with unmodified and modified polymers (PEI2, PEI25 and PAA15) with plasmid DNA at weight ratio 10, as observed by Transmission Electron Microscopy (Philips/FEI (Morgagni)).

#### 5.4.4 *In vitro* Transfection (GFP Expression) Studies

Transfection efficiencies are known to vary greatly among mammalian cell lines principally due to differences in cell physiology, the distribution of cell surface receptors and the uptake pathways used by the cell to internalize complexes (Gersdorff K. et al-2006). Further, immortalized cultured cells such as COS-7, NIH/3T3, HeLa, HEK 293T and CHO cells can be transfected much more readily to higher efficiency than tissue-derived primary cells such as fibroblasts and cord blood mesenchymal stem cells (CB-MS) (Douglas, K.L. et al-2008). The cells are more susceptible to transfection during the process of cell cycle and uptake pathways also make them more susceptible for transfection. In addition, primary tissue-derived cells could be more selective toward the physicochemical properties of the complexes, which can define the predominant endocytic uptake pathway and ultimately how cargos are processed and transported within the intracellular domains (Hsu C.Y.M. and Uludag H-2012). Thus, it is important to note that transfection procedures need to be optimized for individual cell line.

The ability of synthesized gene carriers were evaluated by carrying out gene expression studies with gWIZ-GFP. The gene expression was analyzed by direct measuring

of fluorescence of expressed protein (GFP) in different cell lines using spectrofluorometer. In addition, more accurate cell-by-cell analysis of gene expression was also done using flow cytometry.

#### 5.4.4.1 GFP Expression in 293T Cells by Fluorimetry & Microscopy

Transfection efficiency of ChA conjugates was evaluated in 293T cells using the gWIZ-GFP plasmid to explore the effects of increasing hydrophobicity of native polymers (PEI2 and PEI25). The microscopic images were used to provide direct qualitative analysis of gene expression, whereas, fluorimetry was used for quantitative analysis where fluorescence was measured in arbitrary units. The representative fluorescent microscopy images of PEI2 and PEI25 is presented in figure 5.25.

A general trend of increased transfection efficiency with increase in lipid substitution was observed for both types of polymer conjugates viz PEI2 and PEI25. The PEI2 conjugates (figure 5.24A) were efficient than unmodified PEI2 polymer. It was also noted that a 5 fold increase in mean GFP fluorescence was observed for PEI2-ChA (4) as compared to PEI2-ChA (0.2). PEI25 conjugates also followed same pattern of increased mean GFP fluorescence with increase in lipid substitution (figure 5.24B). Interestingly, for PEI25-ChA conjugates also, the higher lipid substituted conjugate (PEI2-ChA (4)) produced many fold increased GFP fluorescence as compared to its lower substituted counterparts. Therefore, it can be claimed that transfection efficiency was directly proportional to MW of lipid and substitution level of ChA, which is in line with the earlier results of lipid substituted polymers (Incani V. *et al*-2009, Bahadur K. C. *et al*-2011 and Neamark A. *et al*-2009).

In case of PAA15 conjugates, ChA substitution did not increase the transfection efficiency significantly also no general trend was observed as in the case of conjugates of both PEIs and therefore PAA conjugates were not taken for further studies. The relative inefficiency of PAA15 conjugates can be attributed to structural properties of unmodified PAA15, which lacks secondary and tertiary amines. It was also observed that transfection efficiency of polymer conjugates of PEI2 series was increased with increase in polymer/pDNA weight ratio from 3.75 to 30, whereas for PEI25 and PAA15 conjugates, it was decreased after weight ratio 15 and 10, respectively. One of the aspects of an ideal

delivery system for nucleic acids is the ability to bind the DNA tightly to protect it extracellularly and release nucleic acid intracellularly at the site of action (Wang X.L. *et al*-2007). This pattern of decreased transfection of PAA15 conjugate after polymer:pDNA weight ratio 10 can be explained by its inability to dissociate plasmid DNA intracellularly and this can be confirmed by binding and dissociation studies whereby it was found to be tightly bound to pDNA. As far as PEI25-ChA is concerned, decreased transfection after polymer:pDNA weight ratio 15 can be attributed to cytotoxicity of the polymer conjugate at higher weight ratios which decreased overall mean fluorescence.

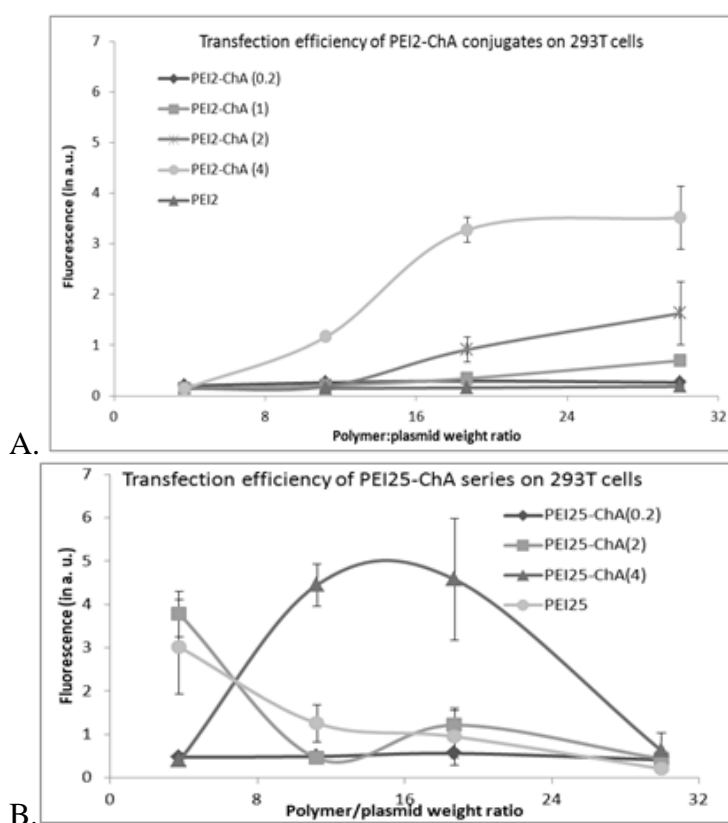


Figure 5.24: Transfection efficiencies of polymer conjugates with different substitution ratios from three different polymer series (A. PEI2, B. PEI25 and C. PAA15) as evaluated in 293T cells using gWIZ-GFP plasmid.

The fluorescent microscopic observation (figure 5.25) also revealed similar trend of increased transfection efficiency with increased lipid substitution and also a direct correlation of increased transfection efficiency with increase in polymer/pDNA weight ratio

from 3.75 to 30 for polymer conjugates of PEI2 and PEI25 series. The PAA15 polymer and its conjugates showed non-significant effect on transfection efficiency, with exception of PAA15-ChA (5) conjugate and that also at polymer/pDNA weight ratio of 10.

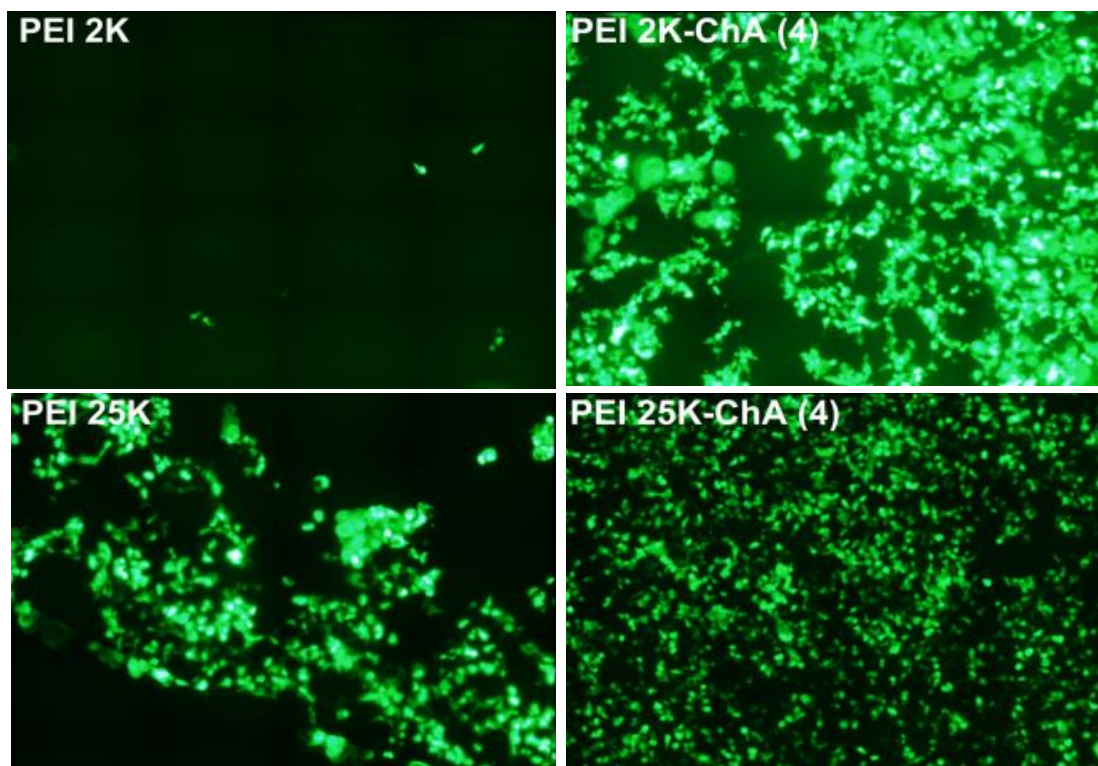


Figure 5.25: Representative fluorescent microscopy images of 293T cells 24 h after treatment of polyplexes of indicated polymers and gWIZ-GFP. The polymer:pDNA ratio was 10 for PEI25 and 15 for all the other polymers.

The polymer/pDNA weight ratio selected for transfection experiment was high as compared to the ratio at which 100% binding was observed (wt ratio ~ 1:1). The excess polycation is needed for improved transfection efficiency (Thibault M. *et al*-2011), but it is also likely the main reason for the observed cytotoxicity. Since the SYBR Green I assay indicated that pDNA binding capacity of PEI25 and PAA15 conjugates remained unaltered as compared to their unmodified counterparts, the reduction on transfection at higher, polymer:pDNA ratios were likely to reflect the cytotoxic effect of the unbound polymers. The PEI2 conjugates, on the other hand, displayed a compromised pDNA binding after substitution so that the proportion of free polymers was probably less at the excess ratio used,

so that no evidence of cytotoxicity was seen for PEI2 conjugates in the experimental range studies. We noted that PAA behaved differently from the PEI polymers since ChA did not seem to affect the transfection efficiency to a significant degree. PAA lack the proton sponge effect typical of PEIs thereby lacking the means to overcome the endosomal escape which is noted to be still significant for lipid substituted polymers.

#### **5.4.4.2 GFP Expression in 293T Cells by Flow Cytometry**

Transfection efficiencies of unmodified polymer (PEI2) and its polymer conjugates (PEI2-ChA) were evaluated in 293T cells using gWIZ-GFP plasmid and GFP expression was analysed 24 h post nanoplexes addition. The data was acquired by flow cytometry and analysis of GFP expression was performed using ModFit 2.0 software (figure 5.26). It was observed that PEI25 and all the polymer conjugates of PEI2 showed higher transfection efficiency at higher polymer:pDNA weight ratio i.e 30 (figure 5.26).

The higher lipid substituted polymer conjugate showed highest transfection efficiency (~68%) in terms of GFP positive cells at higher weight ratio. Moreover, the transfection efficiency of higher lipid substituted polymer conjugate i.e. PEI2-ChA (4) showed highest mean fluorescence intensity (MFI) from GFP positive cells (FL1+) at both the weight ratios used (around 5,000 a.u. of fluorescence). It showed that the higher lipid substituted PEI2 not only transfected more number of cells but yielded more GFP in each cell so as to produce highest MFI of cells from gated region (FL1+ cells) (figure 5.28). It means that PEI2-ChA conjugates have ability to be taken up by large number cell population tested (293T) and the fact that it produces more mean fluorescence implies ability of nanoplexes prepared with PEI2-ChA conjugates to improve overall gene expression of the carried pDNA.

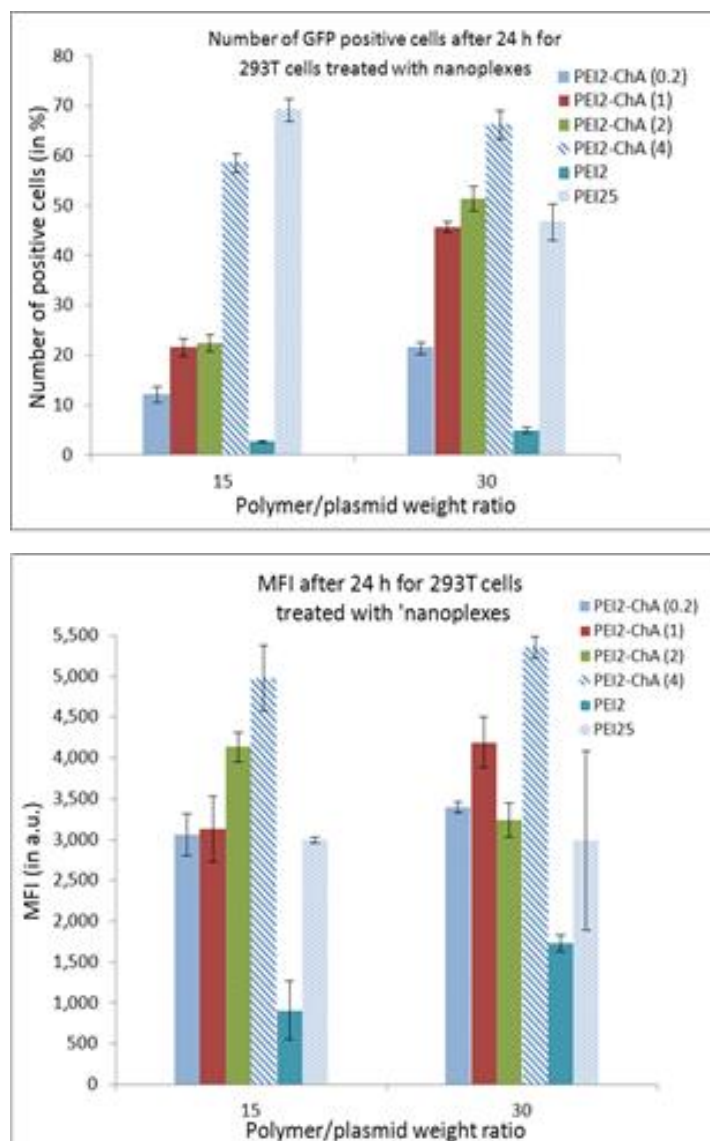


Figure 5.26: Transfection efficiencies of PEI2, PEI25 and PEI2-ChA with different levels of lipid substitution evaluated in 293T cells using gWIZ-GFP plasmid, 24 h post nanoplexes addition.

#### 5.4.4.3 GFP Expression in CB-MSK Cells by Fluorimetry

The GFP expression study for nanoplexes prepared with PEI-ChA conjugates of different ChA substitution levels (lipid:polymer feed ratio of 0.2, 1, 2 and 4) was carried out in CB-MSK cells. As the CB-MSK cells are most primitive cells and are very sensitive to polymer toxicity, lower polymer:pDNA weight ratios were used for the studies with it. The nanoplexes were prepared at different polymer:pDNA weight ratios (3, 5, 10 and 15) in 150 mM saline

and the GFP expression in CB-MSC cells was analysed by using spectrofluorometer. Although the signal was weak (low fluorescence in a.u.), an increased transfection efficiency of PEI2-ChA conjugates at higher substitution can be seen in figure 5.27. In comparison to the nanoplexes prepared with PEI25, PEI2-ChA at higher lipid substitution (i.e. lipid:polymer ratio of 4) produced more fluorescence. It means that PEI2-ChA conjugates work better in terms of transfection efficiency than PEI25.

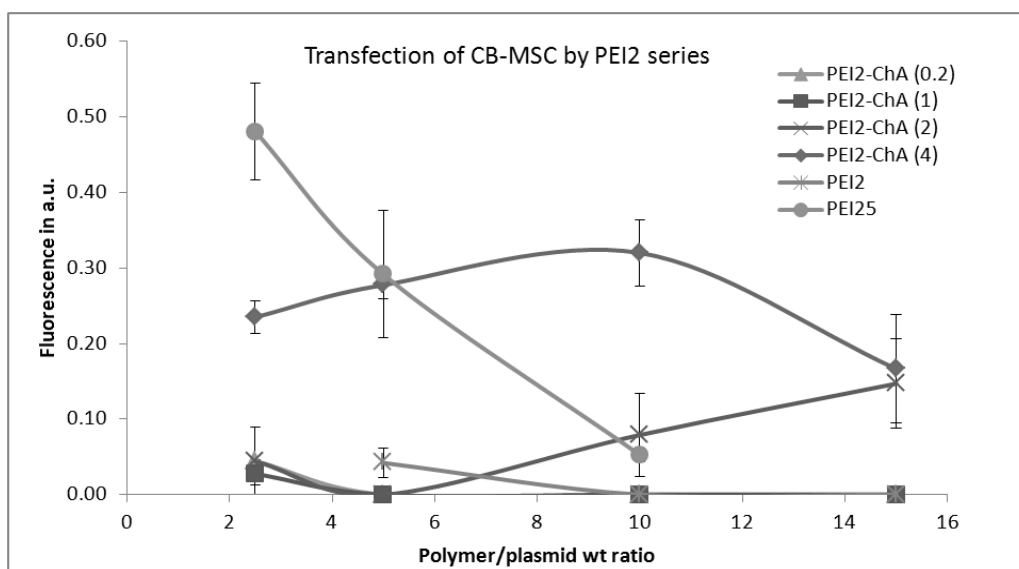


Figure 5.27: Transfection efficiencies of polymer conjugates of PEI2 (PEI2-ChA), as evaluated in 293T cells using gWIZ-GFP plasmid 24 h post nanoplexes addition.

#### 5.4.4.4 GFP Expression in CB-MSC by Flow Cytometry and Microscopy

After demonstrating promising results with transfection of 293T cells, the synthesized polymer conjugates were evaluated in primary CB-MSC. The nanoplexes were prepared at various polymer/pDNA ratios using gWIZ-GFP for CB-MSC transfection. The fluorescent microscopic images (figure 5.28) indicated that transfection efficiency of PEI2-ChA (4) in terms of GFP was significantly higher than its native form (PEI2), which was not effective at all owing to its lower molecular weight and thereby lower amount of primary amines (Shen Y.-2013). Comparable transfection efficiency was obtained with PEI25 and PEI25-ChA.

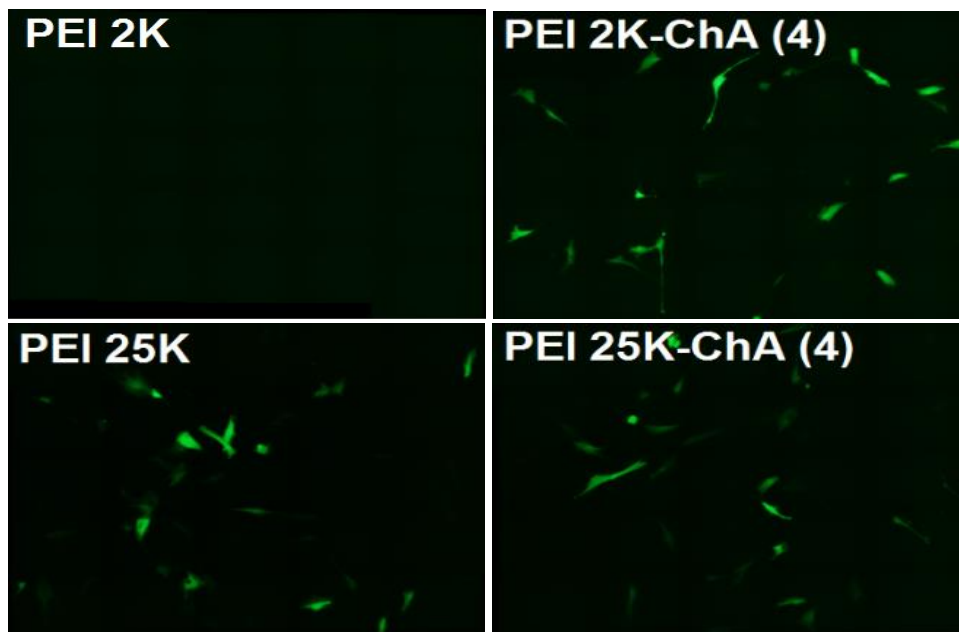


Figure 5.28: Fluorescent images of CB-MSC, 48 after treatment of nanoplexes of polymer or polymer conjugates and plasmid gWIZ-GFP at polymer to plasmid weight ratio 10.

A detailed and quantitative analysis of CB-MSC transfection was then conducted with flow cytometry. Unlike skin fibroblasts (Abbasi M. et al- 2008) and bone marrow stromal cells (Clements B. A. et al- 2009), cellular exposure of plain polymer conjugate solution in saline to CB-MSC did not yield autofluorescence, indicating relatively little toxic effect. The transfection efficiency of low substituted PEI2 conjugates was not significantly different from native PEI2 in terms of mean GFP fluorescence and %GFP-positive cells. Only at the highest ChA (1.9 lipids/PEI2) substitution, a better transfection was evident in terms of mean GFP fluorescence (figure 5.29A) and %GFP positive cells (figure 5.29B). In case of PEI25 conjugates, a similar trend was observed in that higher the substitution level, better the transfection efficiency (figure 5.29D and 5.29E). For PEI25 conjugates, an increasing trend in terms of mean GFP fluorescence was observed even at polymer/plasmid weight ratio of 10, whereas it decreased for unmodified PEI25 after weight ratio of 5. In other words, it can be said that polymer conjugates were significantly more tolerated by the cells as compared to unmodified PEI25. Moreover, it was clear from the graph (figure 5.29F) of cell concentration against polymer/plasmid weight ratio that cytotoxicity of PEI25 conjugates were significantly less than unmodified PEI25. Same is true for PEI2 conjugates (figure 5.29C) which was

significantly less cytotoxic than unmodified PEI25, but PEI2 conjugate with highest ChA (1.9 lipids/PEI2) substitution was significantly more toxic than unmodified PEI2. It can be attributed to increased interaction of the PEI2 conjugate owing to more hydrophobicity imparted by lipid substitution. A slight pattern was observed (figure 5.30) between number of lipids/PEI and transfection efficiency of polymer conjugates in terms of mean GFP fluorescence obtained in CB-MSK for PEI2 conjugates ( $r^2$  value of 0.498) but the pattern was not much clear for PEI25 conjugates ( $r^2$  value of 0.300).

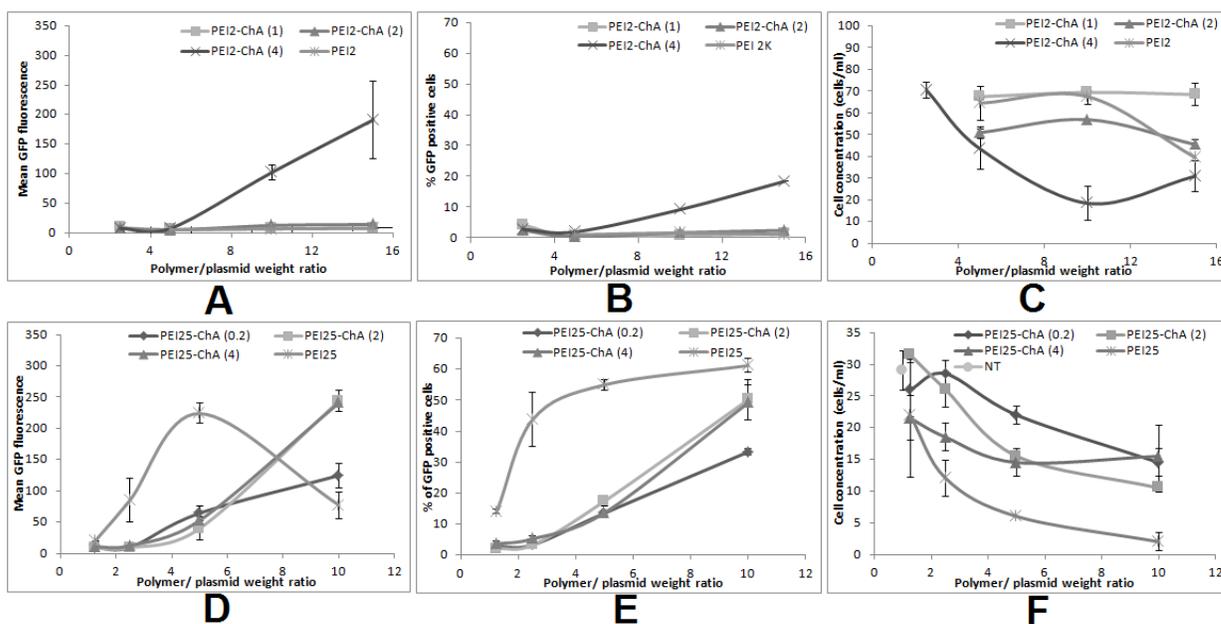


Figure 5.29: Transfection efficiency of nanoplexes prepared with polymer or polymer conjugates with different substitution ratios from two polymer series (PEI2, PEI25) evaluated in CB-MSK using gWIZ-GFP plasmid as analyzed by flow cytometry. Panel A, B and C represents mean GFP fluorescence, %GFP positive cells and cell concentration for PEI2 and its conjugates, whereas panel D, E and F represent same parameters, respectively, for PEI25 and its conjugates.

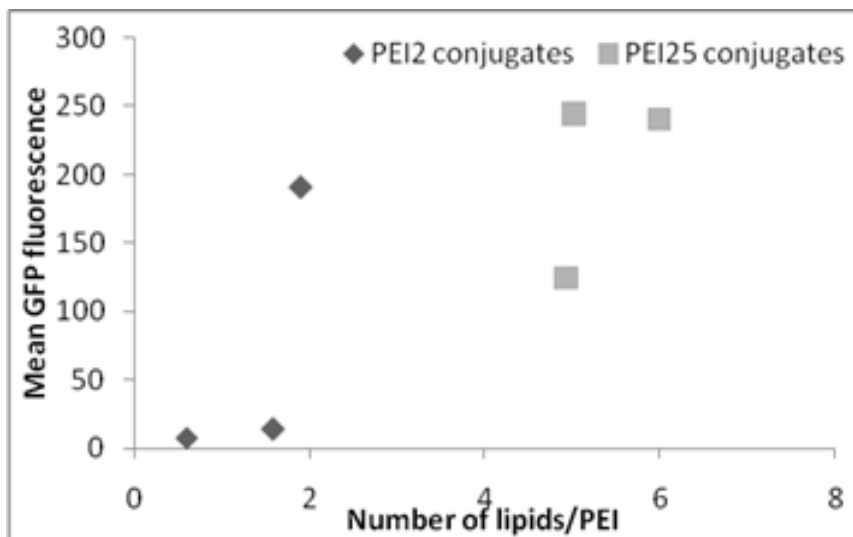


Figure 5.30: Correlation between number of lipids/PEI and transfection efficiency of polymer conjugates in terms of mean GFP fluorescence obtained in CB-MSC using gWIZ-GFP ( $r^2$  value of 0.498 and 0.300 was obtained for PEI2 and PEI25 conjugates, respectively).

#### 5.4.4.5 GFP Expression in U87MG Cells by Flow Cytometry

In pursuit of demonstrating the GFP expression in a brain derived cell line, the transfection efficiency experiment was also carried out in U87MG cell line. Transferrin receptor (TfR) is one of the most attractive targets to overcome the blood-brain-barrier. U87MG cells have been shown to overexpress TfR (Xu G. et al-2011 and Acton Q. A.-2012). Cellular iron uptake is mediated by this ubiquitously expressed receptor for transferrin and it also plays a key role in the control of the rate of cellular iron uptake, tuning the amount of iron delivered to the cells to the metabolic needs (Calzolari A. et al-2010). Therefore, U87MG cell line was chosen to evaluate transfection efficiency of nanoplexes of polymer or polymer conjugates prepared with pDNA and containing transferrin. A quantitative analysis of transfection efficiency of nanoplexes with and without transferrin was carried out in U87MG cells using flow cytometry. Table 5.7 shows treatment groups with corresponding mean %GFP positive cells after normalization.

Table 5.7: Treatment groups of nanoplexes with corresponding mean %GFP positive cells after normalization in U87MG cells.

Sr. No.	Treatment group	Polymer or conjugate:pDNA weight ratio	Tf:pDNA weight ratio	Mean %GFP positive cells after normalization
1	PEI2-ChA	5	5	34.72
2	PEI2-ChA	5	10	43.42
3	PEI2-ChA	12	5	70.41
4	PEI2-ChA	12	10	79.49
5	PEI25-ChA	5	5	77.51
6	PEI25-ChA	12	5	85.62
7	PEI25	4	5	76.58
8	PEI25	8	5	82.76
9	PEI25	8	-	71.51

It was observed that the cellular exposure of control nanoplexes to U87MG did not yield significant autofluorescence which indicates relatively little toxic effect of nanoplexes. As shown in the figure 5.31, the transfection efficiency of PEI2-ChA conjugates at lower polymer:plasmid weight ratio (5) yielded less GFP ( 34.72 %) in the U87MG cell population as compared to PEI2-ChA with higher polymer:plasmid weight ratio (12) which produced 79.41% GFP positive cells (almost double of amount for lower wt ratio). Similar transfection results were also observed in 293T cells and CB-MSCs for nanoplexes of PEI2 and PEI25 series conjugates (for nanoplexes which does not contain transferrin). Moreover, the cells with treatment groups of nanoplexes with conjugates of both the polymer series (PEI2 and PEI25) containing transferrin produced more GFP as compared to the nanoplexes without transferrin (again for both polymer series). A similar trend was also seen for nanoplexes prepared with unmodified PEI25 polymer. Figure 5.32 shows GFP positive and negative cells (shift from gated region) corresponding to different treatment groups with and without transferrin.

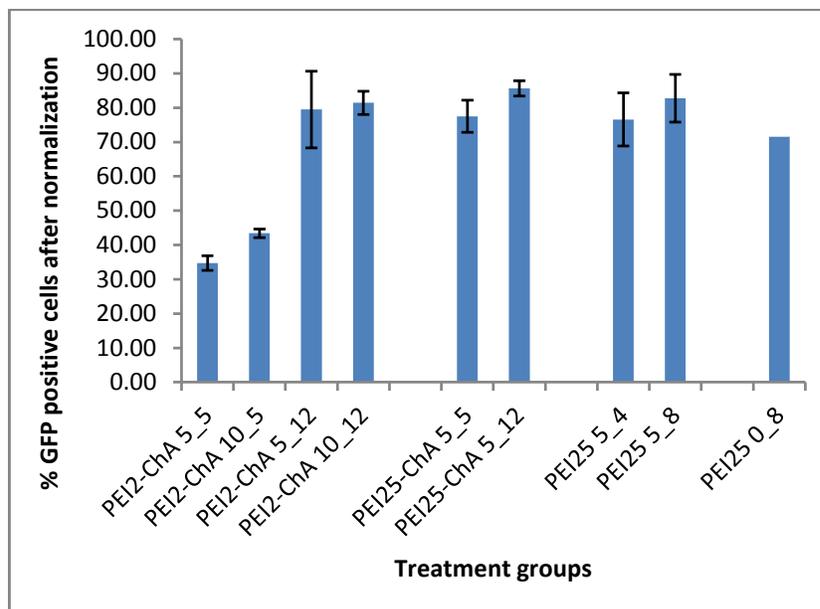


Figure 5.31: The % GFP positive U87MG cells (after normalization) corresponding to different treatment groups with and without transferrin.

It can be also seen that the nanoplexes prepared with unmodified PEI25 polymer but without transferrin showed less GFP expression as compared to the nanoplexes with transferrin. These results were in line with the earlier work of Joshee N et al which showed that their standard formulation, which was prepared by adding DNA to a mixture of transferrin and lipofectin, yielded highest transfection efficiency than the formulation without transferrin (Joshee N et al-2002). An increased transfection efficiency of the nanoplexes can be attributed to the overexpression of TfR on U87MG cells (Acton Q. A.-2012)

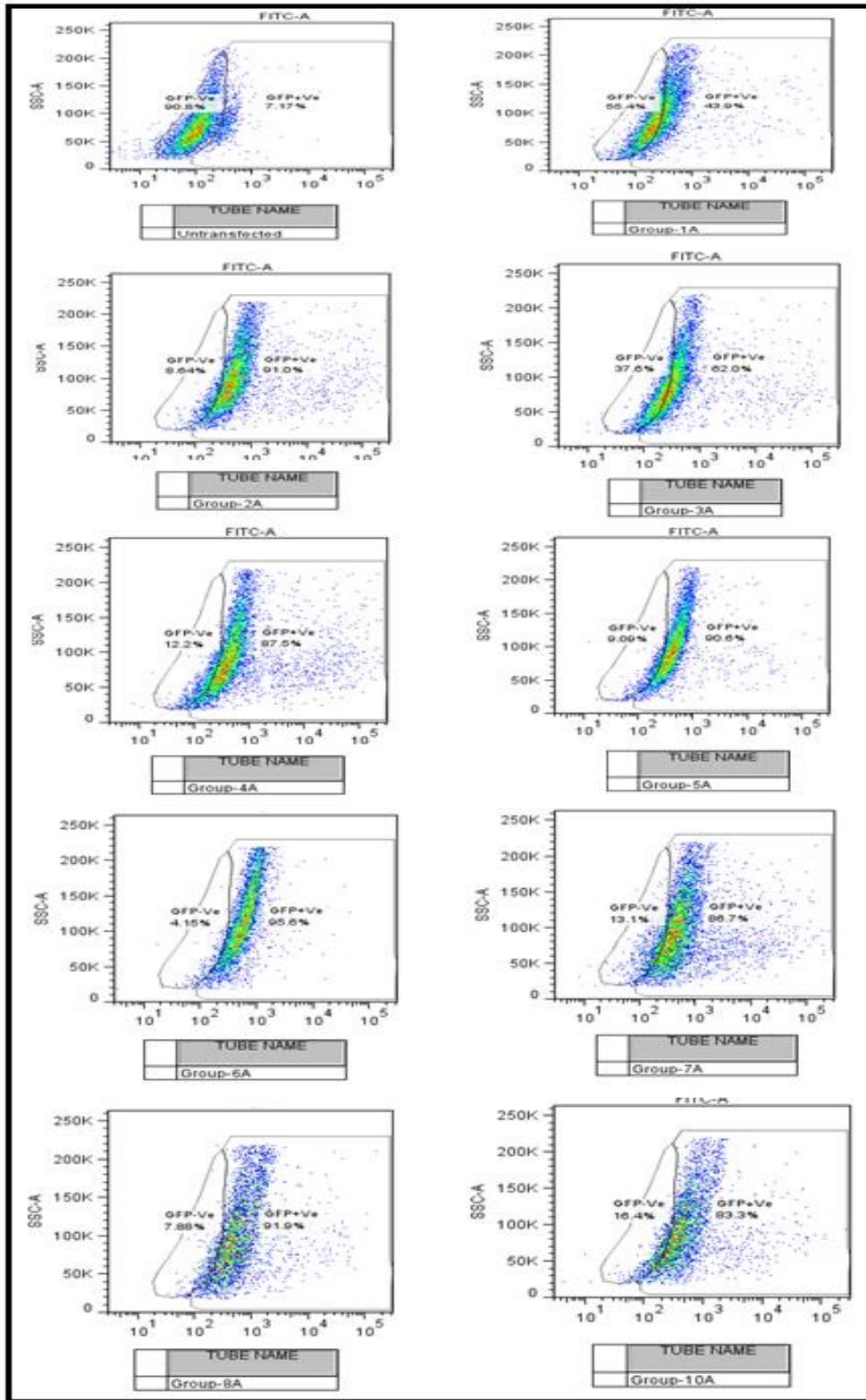


Figure 5.32: Flow cytogram showing GFP positive and negative cells (shift from gated region) corresponding to different treatment groups with and without transferrin.

#### 5.4.4.6 GFP Expression in SKOV3 and NT8e cells by Flow cytometry

After establishing promising transfection efficiency (~80%) of transferrin containing nanoplexes of synthesized polymer conjugate (PEI2-ChA), these polymer conjugates were evaluated for transfection efficiency using pDNA (encoding for p53 tumor suppressor gene) in two cell lines with abnormal p53 status viz. SKOV3 (p53 null) and NT8e cells (p53 mutant). The NT8e cell line was established from human head and neck cancer by group of our research collaborator (Dr. Rita Mulherkar) at Cancer Research Institute, Mumbai and was maintained in the cell medium (Mulherkar R. et al-1997). The cell line grows as a monolayer in vitro and as a transplantable tumor in immune-compromised mice in vivo, and has been used as a model for preclinical studies (Mulherkar R. et al-2010).

The NT8e cell line is also one of the cell lines which are hard to transfect and are more sensitive to the toxicity of polymers. Figure 5.33 shows the typical gating parameters set for the normal NT8e cells based on their volume. As seen in the figure 5.34 the transferrin containing nanoplexes showed transfection of ~25% and ~30 % for polymer:plasmid weight ratio of 10 and 12, respectively. It should be noted from figure 5.34 that the control cells were normalized to ~1% for transfected cells (M2).

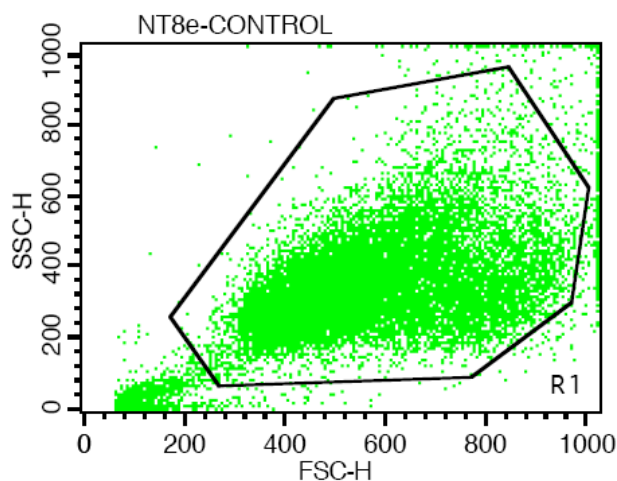


Figure 5.33: Gated region of control cell population for NT8e cells.

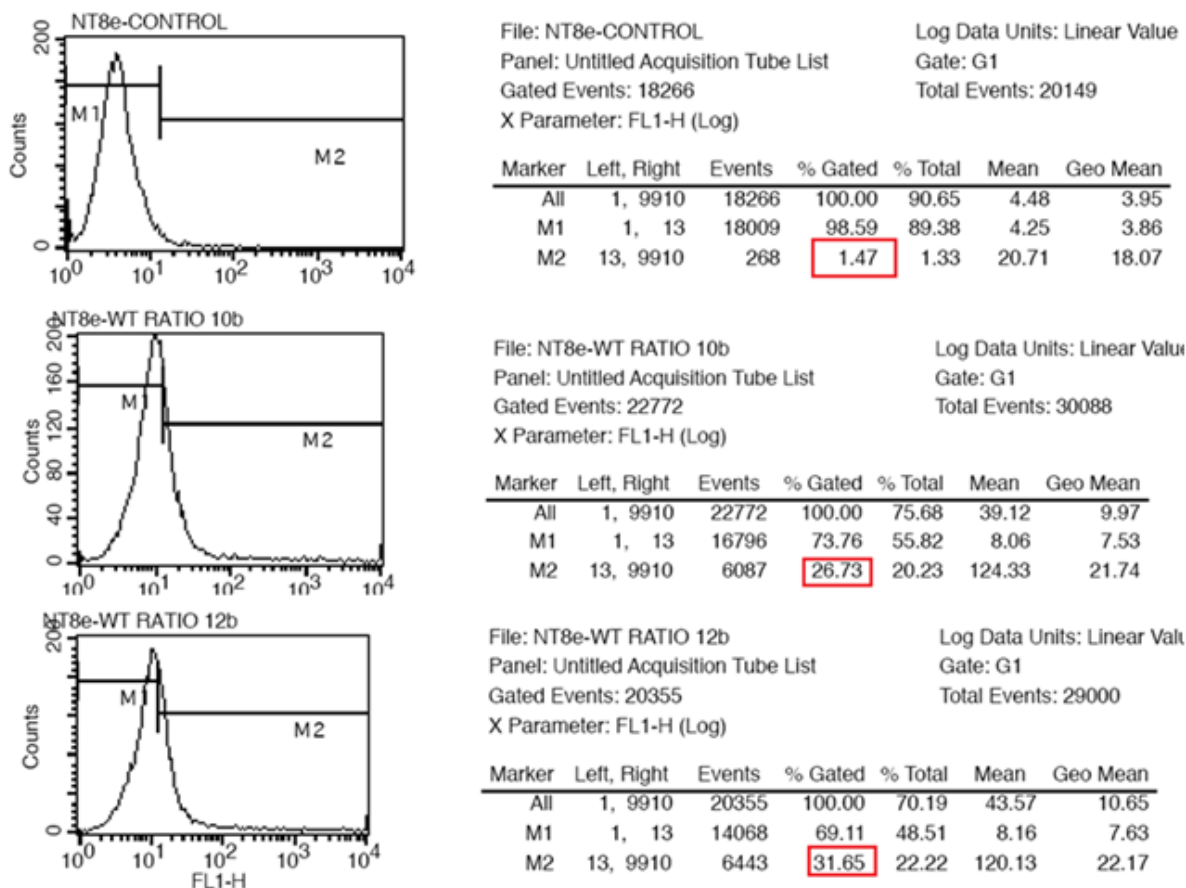


Figure 5.34: GFP expression for nanoplexes prepared in 150 mM saline with polymer to plasmid weight ratio of 10 (B) and 12 (C) in NT8e cells after 48 h by fluorescence microscopy; A is cells treated only with 150 mM saline.

The SKOV-3 cell line is adherent, epithelial, hypodiploid human cell line derived from a 64 years Caucasian female. It should be noted that, according to ATCC literature, SKOV-3 cells are resistant to tumor necrosis factor and to several cytotoxic drugs including diphtheria toxin, cis-platinum and Adriamycin. The cell line grows as a monolayer in vitro and has also been used as a model for preclinical studies.

Figure 5.35 shows the typical gating parameters set for the normal SKOV-3 cells based on their volume. As seen in the figure 5.36, the transferrin containing nanoplexes showed transfection of ~17% and ~19% for polymer:plasmid weight ratio of 10 and 12, respectively. The extent of transfection was similar to that obtained by commercial transfecting agent i.e.

Metafectene (Tsao, S. W. et al-1995). As compared to the NT8e cells, the ~10% less transfection was observed owing to ‘hard to transfect’ nature of this cell line.

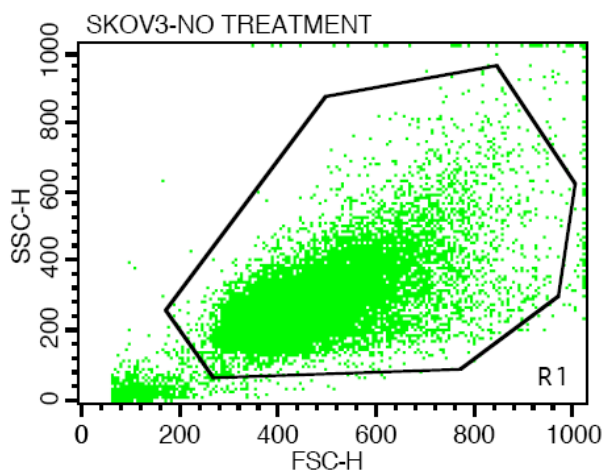


Figure 5.35: Gated region of control cell population for SKOV-3 cells.

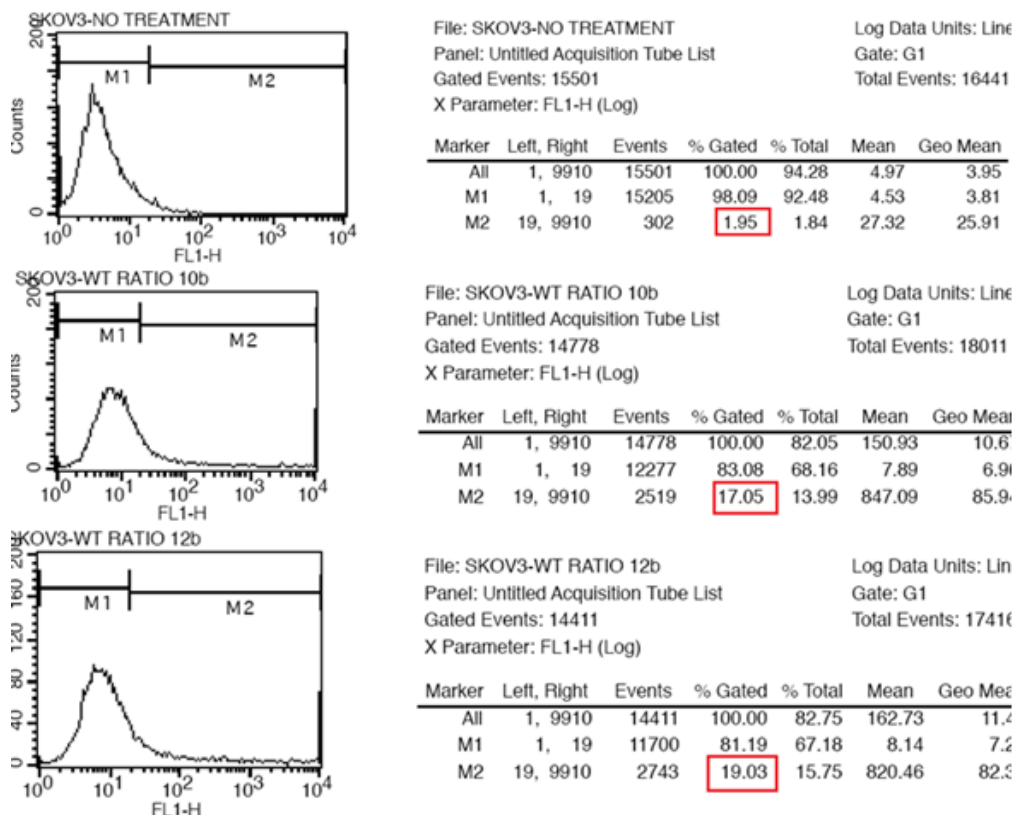


Figure 5.36: GFP expression for nanoplexes prepared in 150 mM saline with polymer to plasmid weight ratio of 10 (B) and 12 (C) in SKOV-3 cells after 48 h by fluorescence microscopy; A is cells treated only with 150 mM saline.

#### 5.4.4.7 GFP Expression in SKOV3 and NT8e cells by Microscopy

The fluorescent microscopic images revealed a similar trend of transfection as observed by flow cytometric analysis for the transferrin containing nanoplexes prepared at two different weight ratios of polymer:pDNA (i.e. 10 and 12) using GFP as reporter gene. But the qualitative evaluation could not show significant difference in transfection efficiency at two different polymer:pDNA weight ratios (fig 5.37).

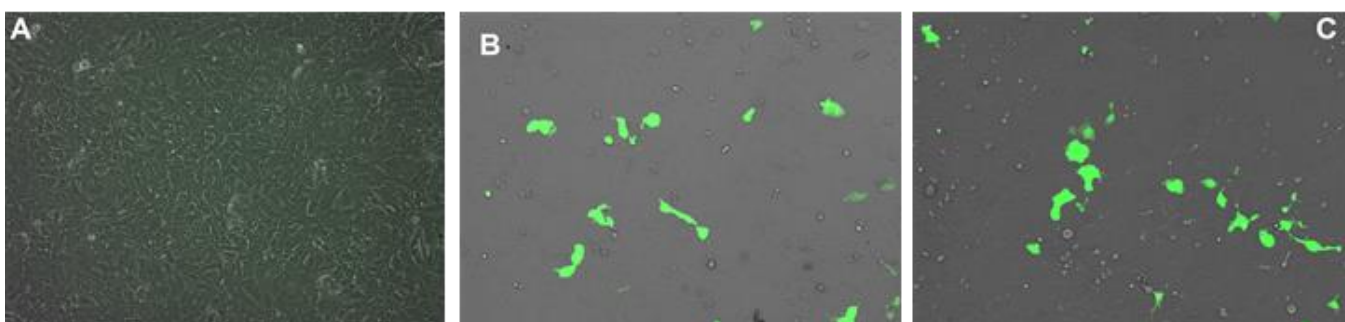


Figure 5.37: GFP expression for nanoplexes prepared in 150 mM saline with polymer to plasmid weight ratio of 10 (B) and 12 (C) in NT8e cells after 48 h by fluorescence microscopy; A is cells treated only with 150 mM saline.

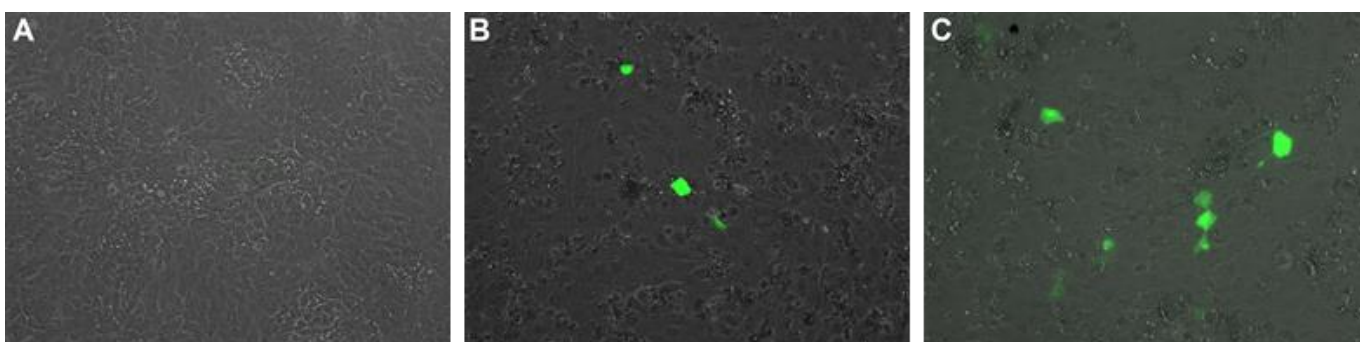


Figure 5.38: GFP expression for nanoplexes prepared in 150 mM saline with polymer to plasmid weight ratio of 10 (B) and 12 (C) in SKOV-3 cells after 48 h by fluorescence microscopy; A is cells treated only with 150 mM saline.

The fluorescent microscopic imaging of SKOV-3 cells revealed lower transfection for the transferrin containing nanoplexes prepared at two different weight ratios of polymer:pDNA (i.e. 10 and 12) using GFP as reporter gene. Although, microscopy is a

qualitative analysis, figure 5.37 implies that the cell line was hard to transfect. However, it appears that qualitative evaluation showed significant difference in transfection efficiency at two different polymer:pDNA weight ratios (Fig 5.38). In other words, it can be stated that higher weight ratios of polymer:pDNA might produce higher transfection in these cells, but again toxicity may become a concern.

#### 5.4.5 Time Dependent Transfection Studies

A time dependent transfection study was carried out to assess the longevity of transfection ability of complexes. Figure 5.39A represents mean GFP fluorescence for PEI2 and its ChA conjugates where only PEI2 conjugate with highest ChA (PEI2-ChA (4) i.e. with 1.9 lipids/PEI2) substitution showed increased mean GFP fluorescence. It should be noted that the y-axis scale was set at higher level to compare the performance of both the polymer conjugates (PEI2 and PEI25 conjugates). A clear decreasing mean fluorescence was observed from day 2 through day 10. Interestingly, graph of %GFP positive cells (figure 5.39B) showed increased % of GFP positive cells on day 4 for PEI2-ChA (4). It could mean that for some population of cells, once the complexes reached inside the cells, the complexes were available for production of encoded protein. But it took 4 days for some of the complexes to produce encoded protein in the other population of cells which became GFP positive only after 4 days. In spite of more GFP positive cells at day 4 than at day 2, the reduced mean GFP fluorescence at day 4 could mean that the GFP produced earlier was not available for fluorescence, because GFP has half-life of 26 hours (Corish P. and Tyler S. C., 1999). This fact can be confirmed by figure 5.39C where difference of mean GFP fluorescence was much clear between day 2 and day 4. PEI25 conjugates also followed same pattern of decreasing mean GFP fluorescence as time progresses (figure 5.39D). It should be noted that only lower polymer:plasmid weight ratio for both PEI25 and its conjugate showed increased % of GFP positive cells at day 4 (figure 5.39E). It can be observed that GFP production was more consistent and sustained as compared to PEI2 conjugate (figure 5.39F). In general, for both the unmodified polymers and polymer conjugates, a clear decreasing trend of transfection was observed as time progressed. Interestingly, mean fluorescence of GFP positive cells for polymer conjugates was higher as compared to unmodified polymers (PEI2 and PEI25). In other words, this could mean that the cells transfected by polymer conjugates produced more

GFP than the cells transfected by unmodified polymer implying that the polymer modification by ChA enhances the transfection efficiency in CB-MSC cells.

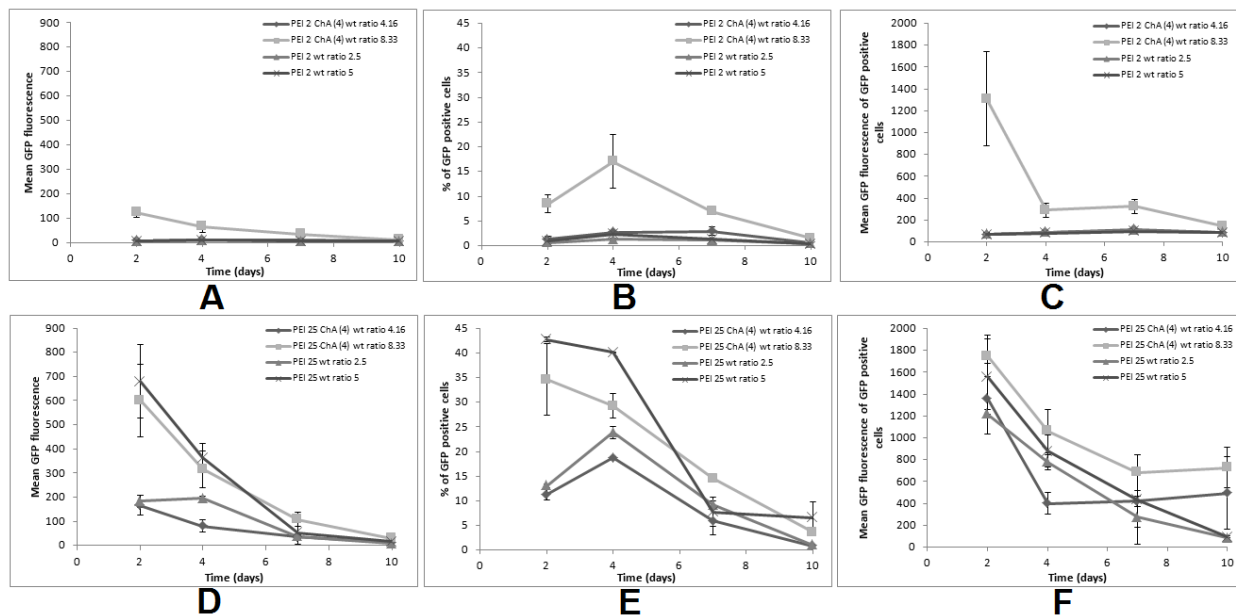


Figure 5.39: Time course study with successful polymer conjugates from PEI2 and PEI25 conjugates as evaluated in CB-MSC using gWIZ-GFP plasmid. Panels A, B and C represents mean GFP fluorescence, %GFP of positive cells and mean GFP fluorescence of GFP positive cells for PEI2 and its conjugates, while panels D, E and F represents the same parameters for PEI25 and its conjugates)

#### 5.4.6 Stability of Nanoplexes

Generally, the complexes (nanoplexes) after formation are unstable in the solution and will gradually form large aggregates over time. It calls for nonviral systems to be used soon after the nanoplexes are formed. In addition, aggregation can occur because of intermolecular charge-charge interaction with serum protein (Luo X.-H. et al.-2011), and/or through interaction with other nanoplexes as a result of hydrophobic shielding. Although, the overall charge of the complex is positive, particles can exist as amphiphatic molecules with pockets of hydrophobic regions (Ikonen, M. et al.-2008); thus, particles may spontaneously bind to each other to shield these hydrophobic pockets from the aqueous solution, forming aggregates. The large aggregates are not desired because of their less efficiency to be taken

up by the cell. Also, such large particles are not as readily dissociated and can lead to increased toxicity, resulting in dramatic reduction in transfection efficiency (Hsu C. M. Y. and Uludag H. -2012). Because of this time sensitivity, complexes are typically incubated with cells for a limited time frame (i.e., <24 h, typically about 2 h).

The transfection efficiency of two treatment groups (i.e group one with no further incubation after preparation and group two with 24 h incubation after preparation); both groups were prepared at at two different weight ratios. These groups were evaluated in 293T cells as shown in figure 5.40. It should be noted that both groups of nanoplexes were added to the cells at the same time.

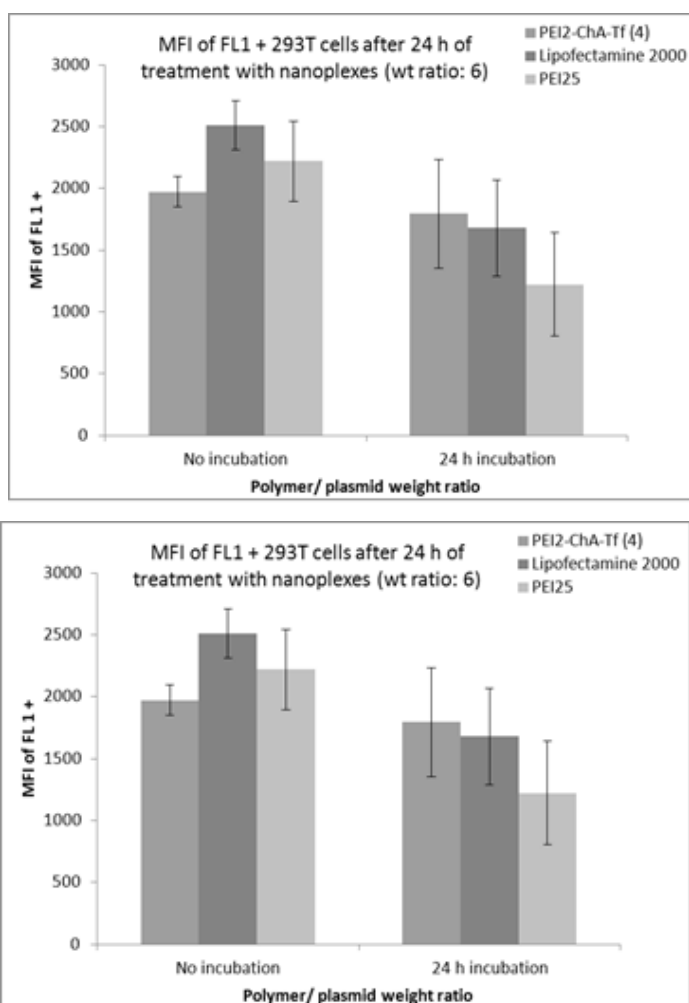


Figure 5.40: Mean fluorescence intensity of FL1+ cells for treatment groups with nanoplexes with 'no incubation' after preparation and '24 h incubation' after preparation (incubation at RT).

The treatment group one (no incubation) nanoplexes were prepared and immediately added to the cells, whereas the nanoplexes with another group (24 h incubation) were prepared 24 h before and added to the cells. A similar transfection trend was observed as obtained with other cell lines (CB-MSK and U87MG) i.e. higher weight ratio nanoplexes showed increased transfection. The figure 5.40 revealed that transfection efficiency of nanoplexes with lipofectamine 2000 (commercially available standard transfecting agent) and PEI25 was decreased after 24 h incubation of the nanoplexes, whereas nanoplexes prepared with PEI2-ChA showed no significant loss of transfection efficiency. These results may be attributed to the fact that transferrin could have played the role in shielding the hydrophobic pockets (formed in the nanoplexes) from the aqueous solution.

#### **5.4.7 BMP-2 Production in hBMSC cells**

The advent of nanotechnology and its use in the production of biomaterials for orthopaedics has led to an increase in interest in its use as a delivery system (Sharma A. et al-2012). As the aim of the present research work was to establish the synthesized polymer conjugates as an efficient transfection agent (nonviral carrier), we evaluated the efficiency of nanoplexes prepared with PEI2-ChA for BMP-2 production. It was clearly visible from figure 5.41 that the nanoplexes with PEI2-ChA at polymer/plasmid (BMP-2) weight ratio of 4:1 and 16:1 ratio led to increased BMP-2 production compared to the nanoplexes prepared with PEI25 at 4:1 or 2:1 weight ratio. Under the microscope after visual inspection, PEI25 showed higher toxicity even at the lowest concentration (2:1) whereas much less cytotoxicity was observed at highest ratio (16:1) of PEI2-ChA. The hBMSC cells are more sensitive and hence PEI25 causes more toxicity to it even at lower weight ratios.

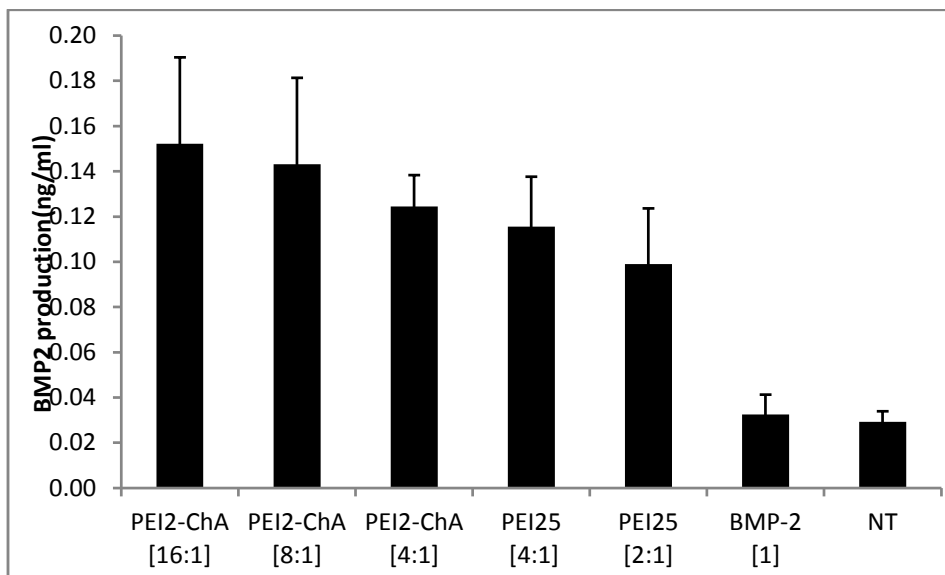


Figure 5.41: BMP-2 production in hBMSC cells using the nanoplexes prepared with PEI2-ChA and PEI25. No treatment group was used as a control (with 150 mM saline) and plasmid BMP-2 group was used as negative control.

#### 5.4.8 pDNA (pp53) digestion study

The isolated plasmid DNA encoding p53 gene (pCMV-NEO-BAM) was confirmed its p53 insert by restriction enzyme (pDNA digestion) study using *EcoRI* and *BamHI* restriction enzymes. After digestion by restriction enzymes the reaction mixture was run on 0.8% agarose gel which showed two type of fragments viz. 4.8 kb of linearized vector and 1.8 kb of p53 insert (figure 5.42). It should be noted that the size of pCMV-NEO-BAM was 6.6 kb.

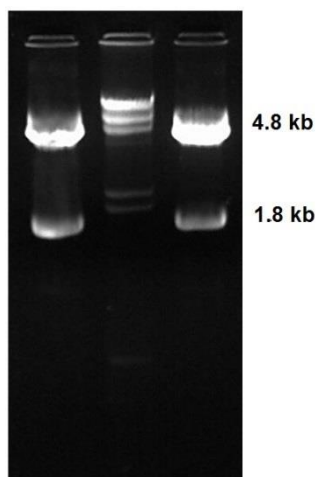


Figure 5.42: Gel electrophoresis image showing p53 insert.

### 5.4.9 Cell cycle analysis in NT8e cells

Apoptosis is a crucial mechanism in eliminating cells with unrepaired DNA damage and preventing carcinogenesis. It is characterized by a p53-dependent induction of pro-apoptotic proteins, leading to permeabilization of the outer mitochondrial membrane, release of apoptogenic factors into the cytoplasm, activation of caspases and subsequent cleavage of various cellular proteins (Fragkos M. and Beard P.- 2011). Apoptogenic effects include chromatin condensation and exposure of phosphatidylserine on membrane surfaces of the cell (Meier P. and Vousden K.H.- 2007). It has been suggested that p53-independent mechanisms of killing tumor cells may not involve apoptosis and could be a result of induced mechanical damage, rather than programmed cell death (Finkel E.-1999). The transferrin incorporated nanoplexes of PEI2-ChA with plasmid p53 showed increased apoptosis in NT8e cells (figure 5.43). The increased apoptosis clearly suggested restored p53 function. Table 5.8 shows that p53 in saline solution has similar effect as that of control samples. Also, it can be seen from the table that solutions of polymer conjugate (PEI2-ChA and PEI25-ChA) corresponds to low apoptosis values indicating that they does not contribute to the apoptosis. In other words, the apoptosis is sole due to delivery of plasmid p53 into the cell and thereby restoration of p53 protein.

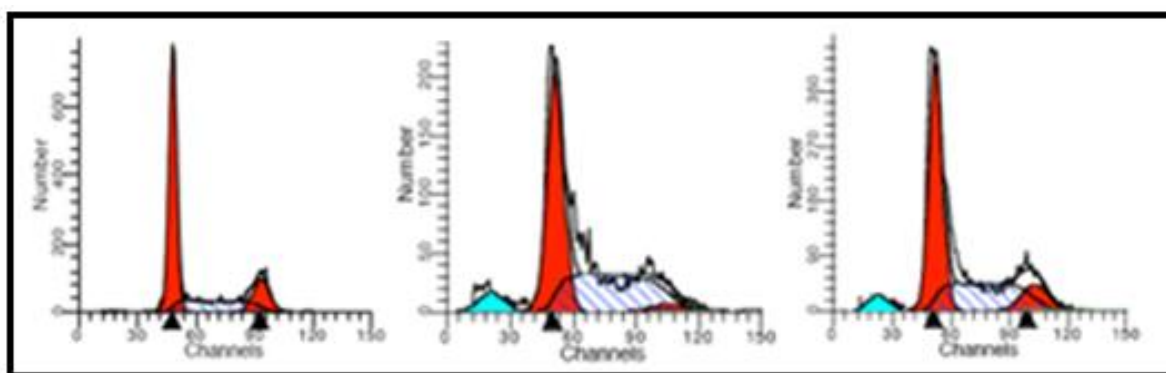


Figure 5.43: Cell cycle analysis in NT8e cells showing cell population corresponding cell cycle phases (G0-G1, G2-M and S phases)

Table 5.8: Cell cycle analysis in NT8e cells

Sr. No.	Group	G0-G1	S	G2-M	Apoptosis
1	Control (saline)	86.70	6.79	6.51	4.38
2	PEI2-ChA-Tf (wt ratio 8)	65.02	30.67	4.31	9.52
3	PEI2-ChA-Tf (wt ratio 10)	65.76	30.27	3.96	<b>22.29</b>
4	PEI2-ChA	65.38	30.94	3.68	5.92
5	PEI25-ChA-Tf (wt ratio 4)	86.01	7.71	6.27	<b>23.44</b>
6	PEI25-ChA-Tf (wt ratio 8)	59.09	37.95	2.96	7.10
7	PEI25-ChA	69.96	27.55	2.47	3.60
8	p53 in saline	86.59	7.54	5.87	<b>4.87</b>

### 5.5 *In vitro* protein expression studies

The total protein of all samples of cell lysates was estimated by Lowry's protein estimation assay. A calibration curve was plotted for standard BSA solution from 6 to 36  $\mu\text{g/ml}$  in distilled water against absorbance at 600 nm. The plot showed linear correlation between amount of protein and absorbance with  $r^2$  value of 0.998 as shown in figure 5.44 and the values obtained are shown in table 27.

Table 5.9: Calibration plot of BSA by Lowry's protein estimation assay

Sr. No.	BSA ( $\mu\text{g}/250 \mu\text{l}$ )	Mean
1	0	-
2	6	0.068
3	12	0.1285
4	18	0.167
5	24	0.217
6	36	0.3195

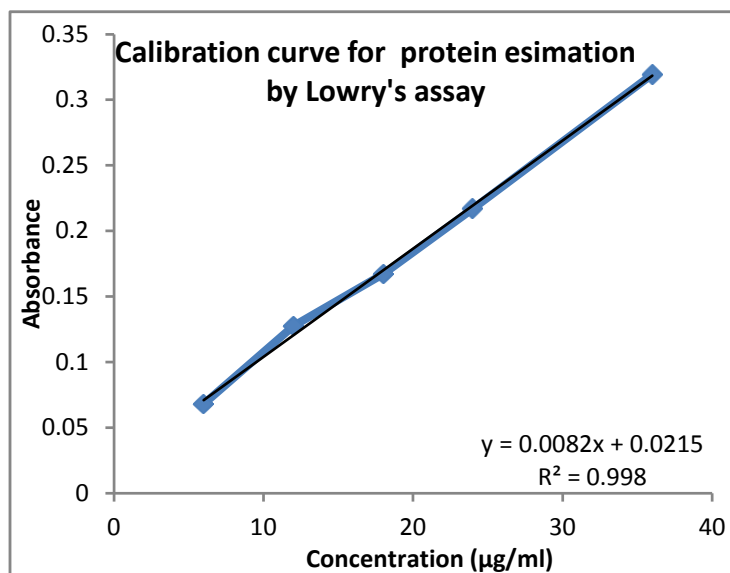


Figure 5.44: Calibration curve of BSA by Lowry's protein estimation assay.

Table 5.10: Treatment groups for protein expression studies of p53 in two different cell lines (i.e. NT8e and SKOV-3 cells). PEI25 was used as positive control and naked pDNA as negative control.

Sr. No.	Treatment	Mean	Actual quantity (µg/ml)
<b>NT8e Cell samples</b>			
1	PEI2-ChA-Tf (wt ratio 8)	0.2355	26.05
2	PEI2-ChA-Tf (wt ratio 10)	0.249	27.70
3	PEI25 (wt ratio 5)	0.219	24.04
<b>SKOV-3 Cell samples</b>			
4	PEI2-ChA-Tf (wt ratio 8)	0.12	11.96
5	PEI2-ChA-Tf (wt ratio 10)	0.1205	12.02
6	PEI25 (wt ratio 5)	0.0975	9.22

The p53 tumor suppressor protein is involved in several central cellular processes that are critical for maintaining cellular homeostasis, including gene transcription, DNA repair, cell cycling, senescence, and apoptosis (Vogelstein B. and Kinzler K.W.-1992 and Levine A.J.-1997). But compared with the vast information and knowledge available regarding the

role of p53 protein in apoptosis, the function of p53 in cell differentiation is not well understood (Liu J. et al-1999). It was imperative to analyze the p53 gene expression before proceeding for in vivo animal studies.

Although, western blot analysis is semiquantitative, it was clearly seen from the figure 5.45 that p53 was expressed significantly more in NT8e cells in comparison with the p53 expression in SKOV-3 cells. The NT8e is a p53 mutant cell line which contains its endogenous mutant p53, therefore these cells showed two bands for p53 i.e. one for endogenous p53 and another for exogenous p53 protein. The relatively less expression in lane 3 was of PEI25 which was used as positive control. The naked plasmid p53 (lane 2) and only saline solution i.e. no treatment were used as negative controls. It appeared that there wasn't any significant difference between treatment groups of weight ratio 8 and 10 for SKOV-3 cell line (figure 5.45B). But there was a significant difference between treatment groups of weight ratio 8 and 10 as observed visually (figure 5.45A) for NT8e cell line. It should be noted that an equal loading of protein samples was clearly seen from  $\beta$  tubulin expression in both the cell lines.

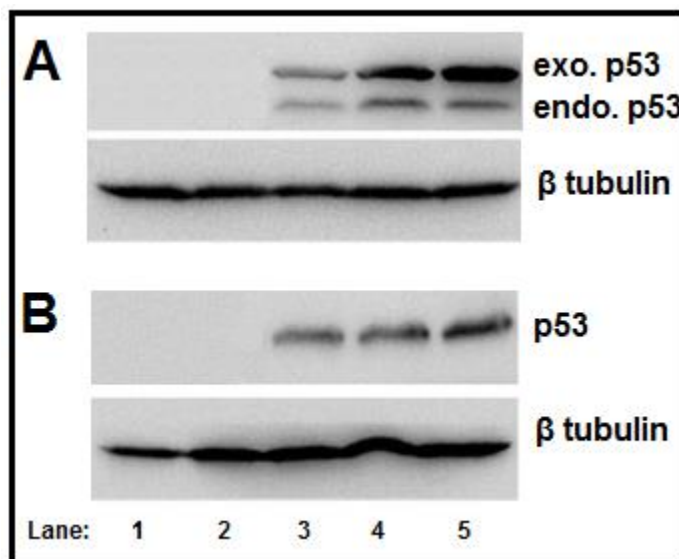


Figure 5.45: The p53 protein was harvested (25  $\mu$ g) and analyzed for the expression by western blot analysis using anti-mouse primary antibody p53 in NT8e cells (A) and SKOV-3 cells (B).

## 5.6 Biodistribution Studies

The fluorescence imaging uses an external light source to excite a variety of fluorescent compounds, the most common of which is green fluorescent protein (GFP). Structurally, GFP is a beta barrel with a centrally located tripeptide sequence undergoing cyclization reactions in the presence of oxygen to serve as the chromophore (Yang F. et al-1996). The chromophore emits green light at a wavelength of 509 nm when exposed to an excitation peak of 395 nm (blue light). Imaging with GFP has previously been used to study the gene expression in hESCs (Vallier L. et al-2004). Although bioluminescence is favored for gene expression over fluorescence as far as organ depth is concerned, using longer wavelength fluorescent proteins may improve tissue penetration depth.

In vivo imaging of mice treated with nanoplexes of PEI2-ChA without transferrin (figure 5.46A, B & C) and with transferrin (figure 5.46D, E & F) is shown in figure 5.47. Control mouse (figure 5.46G) was treated only with 150 mM saline. The epi-fluorescence scale showed that the highest fluorescent intensity signal appears as yellow color in all the images. The red color is either autofluorescence or weak GFP signal. It can be clearly seen from figure 5.46 that animals injected intravenously with transferrin containing nanoplexes prepared with PEI2 conjugates (PEI2-ChA-Tf) showed localized yellow colored signal (highest GFP intensity) in brain region (figure 5.46D, E and F). It should be noted that the GFP signal was spotted only in brain region which implied that it was a GFP signal and not an autofluorescence. Moreover, autofluorescence was associated with red color which was not the case as far as brain region is concerned. The animals injected with the nanoplexes without transferrin prepared with PEI2 conjugates (PEI2-ChA-Tf) showed strong GFP expression in lung region (figure 5.46A and B), but weak GFP signals in lung area (figure 5.46C).

In addition to in vivo imaging, ex vivo imaging for organs isolated from animals treated with and without transferrin was also carried out as shown in figure 5.46H while figure 5.46I showed the images of the same organs in plain bright light. The organs from the animals injected with transferrin containing nanoplexes clearly showed a strong signal for GFP in brain, whereas only weak signal was seen in brain and lung for the nanoplexes without transferrin. Thus it can be concluded that transferrin containing nanoplexes has ability to carry therapeutic gene to brain region and thereby in brain tumors.

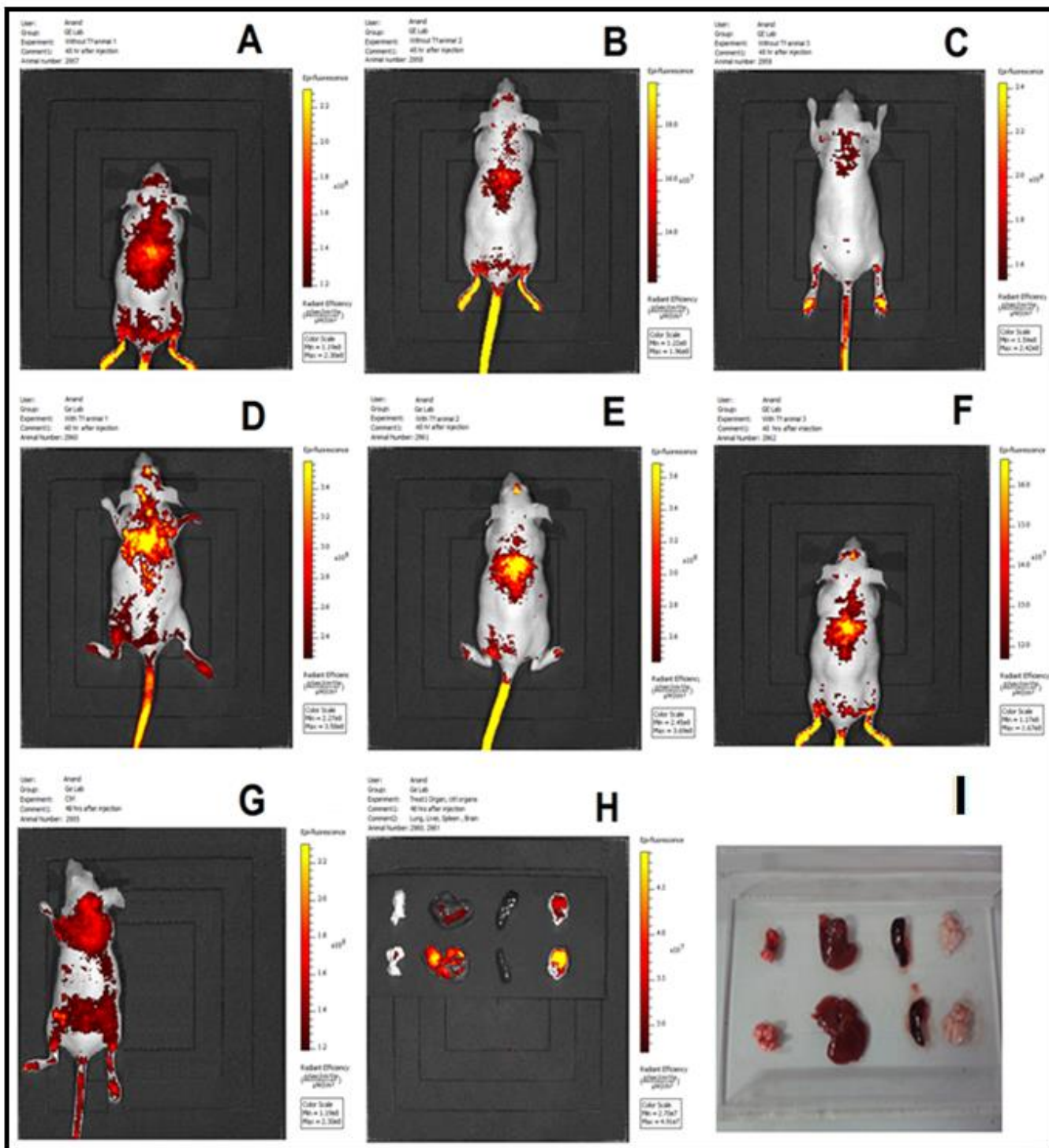


Figure 5.46: In vivo imaging of mice treated with nanoplexes of PEI2-ChA without transferrin (A, B & C) and with transferrin (D, E & F). Control mice (G) were treated only with 150 mM saline. H & I are images for organs isolated from animals treated with and without transferrin.

In addition to imaging in IVIS imaging system (Xenogen, USA), few images were taken in plain bright light and UV light directly (figure 62A and B). The GFP signal for transferrin containing nanoplexes prepared with PEI2 conjugates (PEI2-ChA-Tf) was so high in brain and lung region that it can be clearly visualized in direct UV light. It further supports the results obtained by whole animal imaging in IVIS Lumina (figure 61).



Figure 5.47: Bright light (A) and UV light (B) images of organs isolated from the mouse treated with transferrin containing nanoplexes of polymer conjugate (PEI2-ChA) with pDNA.

### 5.7 Tumor Regression Studies

Tumor regression is an improvement or cure from a disease that appears to be progressing in its severity (Xue W. et al-2007). The tumor regression could occur by apoptosis (programmed cell death) and/or by anti-angiogenic effects (growth of new blood vessels) of therapeutic agents. Treatment with wild-type plasmid p53 induces regression of ectopic solid tumors. Pictures in the figure 5.48 show tumor volume of untreated/control mice (figure 5.48A) and mice treated with transferrin containing nanoplexes of PEI2-ChA with plasmid p53 (figure 5.48B). The numbers in the pictures denotes in-house animal numbers for identification and are unique for each animal. Tumors were allowed to progress without intervention for 48 days post-tumor induction. Animals were treated with 8  $\mu\text{g}$  of plasmid p53 in transferrin containing nanoplexes of PEI2-ChA per animal or the vehicle control (150 mM saline solution) resulting in treatment for 48 days.

At 48 days post-tumor induction, p53 treated tumors were significantly smaller compared with control animals as shown in figure 5.48 and 5.50. The tumors of untreated mice were ~5 times bigger in size than the tumor of animals treated with transferrin containing nanoplexes of PEI2-ChA (table 5.11 and 5.12).

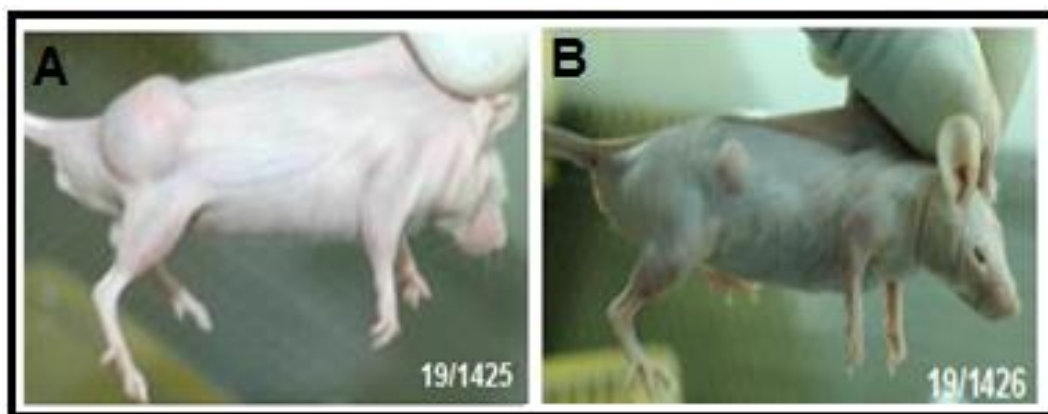


Figure 5.48: Treatment with wild-type plasmid p53 induces regression of ectopic solid tumors. Pictures showing tumor volume of untreated/control mice (B) and mice treated with transferrin containing nanoplexes of PEI2-ChA with plasmid p53 (A). The numbers in the pictures denotes in-house animal numbers for identification and are unique for each animal.

Table 5.11: Tumor size of control group at tumor induction and post-tumor induction (cm<sup>3</sup>)

Mouse No.	Tumor size of control group at tumor induction			Tumor size of control group post-tumor induction		
	length (cm <sup>3</sup> )	width (cm <sup>3</sup> )	tumor volume (cm <sup>3</sup> )	length (cm <sup>3</sup> )	width (cm <sup>3</sup> )	tumor volume (cm <sup>3</sup> )
19/1424	0.772	0.480	0.089	1.062	0.902	0.432
19/1425	0.768	0.650	0.162	1.136	0.838	0.399
19/1430	0.670	0.575	0.111	0.812	0.880	0.314
19/1433	0.724	0.576	0.120	1.016	0.798	0.323
19/1437	0.735	0.680	0.170	1.135	1.038	0.611

Table 5.12: Tumor size of treated group before and after treatment (cm<sup>3</sup>)

Mouse No.	Tumor size of treated group BEFORE treatment			Tumor size of treated group AFTER treatment		
	length (cm <sup>3</sup> )	width (cm <sup>3</sup> )	tumor volume (cm <sup>3</sup> )	length (cm <sup>3</sup> )	width (cm <sup>3</sup> )	tumor volume (cm <sup>3</sup> )
19/1422	0.685	0.56	0.107	0.487	0.465	0.053
19/1426	0.766	0.548	0.115	0.651	0.415	0.056
19/1427	0.694	0.505	0.088	0.551	0.399	0.044
19/1429	0.751	0.68	0.173	0.589	0.464	0.063
19/1434	0.684	0.533	0.097	0.511	0.568	0.082

Figure 5.49 shows the tumor size of two groups (termed as control and treated) after tumor induction (cm) and figure 5.50 shows tumor size of control and treated group after treatment (cm) ( $p < 0.001$ ). It was shown in the cell cycle analysis that the cell kill was majorly due to apoptosis of cancerous cells, which contributed to the regression of tumors in the present work. Thus, it can be concluded that the cholic acid modified PEI2 conjugates (i.e. PEI2-ChA) can be effectively used towards regression of brain tumors in humans after exhaustive preclinical studies are carried out.

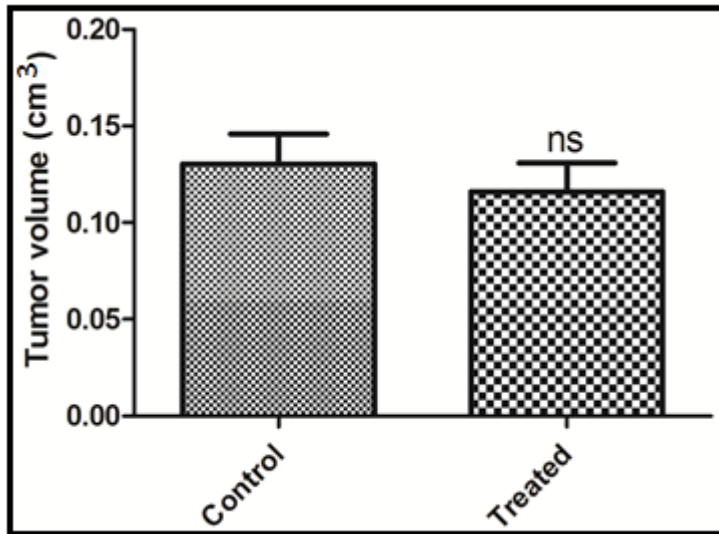


Figure 5.49: Tumor size of two groups (termed as control and treated) after tumor induction (cm).

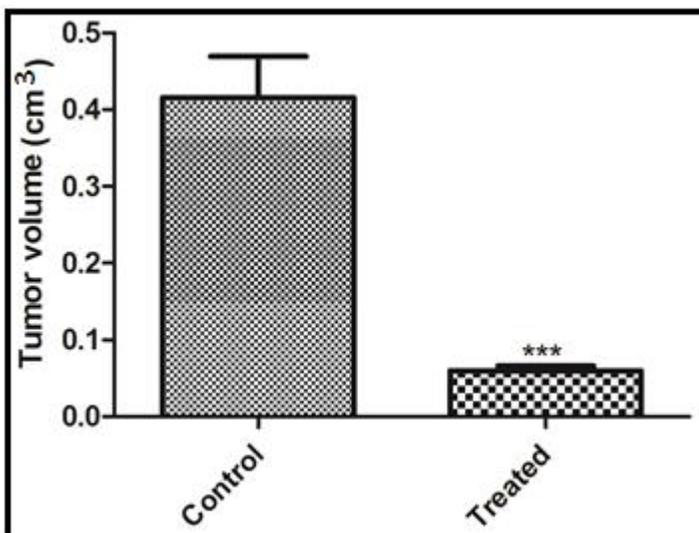


Figure 5.50: Tumor size of control and treated group after treatment (cm) ( $p < 0.001$ )

**REFERENCES**

- Al-Deena F.N., Selomulyaa C., Williams T., On designing stable magnetic vectors as carriers for malaria DNA vaccine, *Colloids and Surfaces B: Biointerfaces*, 2013;102: 492– 503.
- Bahadur K.C., Landry B., Aliabadi H.M., Lavasanifar A., Uludag H., Lipid substitution on low molecular weight (0.6–2.0 kDa) polyethylenimine leads to a higher zeta potential of plasmid DNA and enhances transgene expression, *Acta Biomaterialia* 7., 2011; 2209–2217.
- Calzolari A., Luigi Maria Larocca., Roberto Pallini., Transferrin Receptor 2 Is Frequently and Highly Expressed in Glioblastomas, *Transl Oncol.*, 2010; 3 (2): 123-34.
- Darr A., Calabro A., Synthesis and characterization of tyramine based hyaluronan hydrogels, *J Mater Sci: Mater Med.*, 2009; 20: 33-44.
- Du Y, Cai L, Li J, Zhao M, Chen F, Yuan H, Hu F, Receptor-mediated gene delivery by folic acid-modified stearic acid-grafted chitosan micelles, *International Journal of Nanomedicine*, 2011; 6: 1559-1568.
- Finkel E., Does cancer therapy trigger cell suicide?, *Science*, 1999; 286: 2256–2258.
- Fragkos M. and Beard P., Mitotic Catastrophe Occurs in the Absence of Apoptosis in p53-Null Cells with a Defective G1 Checkpoint., *PLoS ONE* 6(8): e22946.
- *Functional Polymers for Nanomedicine*, Edited by Shen Y., Royal Society of Chemistry, 2013, Chapter 4, 66.
- Gratton S.A., Ropp P.A., Pohlhaus P.D., Luft J.C., Madden V.J., Napier M.E., The effect of particle design on cellular internalization pathways, *Proc Natl Acad Sci, U S A*. 2008; 105:11613-8.
- Grzelczak M., Vermant J., Furst E.M., Liz-Marzan L.M., Directed self-assembly of nanoparticles, *ACS Nano.*, 2010; 4:3591-605.
- Hermanson G.T. *Bioconjugate Techniques*, 2<sup>nd</sup> ed, Academic Press, Salt Lake, UT, USA. 2008.
- Hoffmann C., Faure A.C., Vancaeyzeele C., Roux S., Tillement O., Pauthe E., Goubard F., Labeling of fibronectin by fluorescent and paramagnetic nanoprobe for

- exploring the extracellular matrix: bioconjugate synthesis optimization and biochemical characterization, *Anal Bioanal Chem.*, 2011; 399:1653-63.
- Ikonen M., Murtomäki, L., Kontturi K., Controlled complexation of plasmid DNA with cationic polymers: effect of surfactant on the complexation and stability of the complexes, *Colloids Surf B Biointerfaces.*, 2008; 66: 77–83.
  - Incani V., Lin X., Lavasanifar A., Uludag H., Relationship between the Extent of Lipid Substitution on Poly(L-lysine) and the DNA Delivery Efficiency, *Applied Materials and Interfaces.*, 2008; 1: 841–848 .
  - Joshee N., Bastola D.R, Cheng P.W., Transferrin-facilitated lipofection gene delivery strategy: characterization of the transfection complexes and intracellular trafficking., *Hum Gene Ther.* 2002;13:1991-2004.
  - Kopatz I., Remy J.S., Behr J.P., A model for non-viral gene delivery: through syndecan adhesion molecules and powered by actin, *J Gene Med.*, 2004; 6: 769-76.
  - Levine A.J., p53, the cellular gatekeeper for growth and division., *Cell*; 1997; 88: 323-31.
  - Liu J.n., Cong Li., Thomas E., Ahlborn, Michael J. Spence., Lou Meng., Linda M. Boxer., The Expression of p53 Tumor Suppressor Gene in Breast Cancer Cells Is Down-Regulated by Cytokine Oncostatin M1, *Cell Growth & Differentiation.*, 1999;. 10: 677-683.
  - Luo, X.-H. et al. A strategy to improve serum-tolerant transfection activity of polycation vectors by surface hydroxylation, *Biomaterials.*, 2011; 32: 9925–9939.
  - Meier P, Vousden KH (2007) Lucifer's labyrinth - ten years of path finding in cell death. *Mol Cell* 28: 746–754
  - Moret I., J. Esteban Peris., V. M. Guillem, M. Benet, F. Revert, F. Dasi, A. Crespo, and S. F. Alino.. Stability of PEI-DNA and DOTAP-DNA complexes: effect of alkaline pH, heparin and serum. *J. Control Release.* 2001; 76:169–181.
  - Mulherkar R., Gene and cell therapy in India, *Current Science*, 2010; 99 (11): 1542-48.

- Mulherkar R., Goud A.P., Wagle A.S., Naresh K.N., Mahimkar M.B., Thomas S.M., Establishment of a human squamous cell carcinoma cell line of the upper aerodigestive tract, *Cancer Lett* 1997; 118: 115-21.
- Nakajima N., Ikada Y., Mechanism of amide formation by carbodiimide for bioconjugation in aqueous media, *Bioconjugate Chem.*, 1995; 6: 123-130.
- Neamark A., Suwantong O., Bahadur K.C., Hsu C.Y.M., Supaphol P., Uludag H., Aliphatic lipid substitution on 2 kDa polyethylenimine improves plasmid delivery and transgene expression, *Mol Pharm.*, 2009; 6: 1798–815
- Neu M., Sitterberg J., Bakowsky U., Kissel T., Stabilized nanocarriers for plasmids based upon cross-linked poly(ethylene imine)., *Biomacromolecules.*, 2006;7: 3428-38.
- Ogris M., Steinlein P., Kursa M., Mechtler K., Kircheis R. Wagner E., The size of DNA/transferrin-PEI complexes is an important factor for gene expression in cultured cells, *Gene Therapy* (1998) 5, 1425–1433.
- Sharma A., F. Meyer., M. Hyvonen., S. M. Best., R. E. Cameron., N. Rushton., Osteoinduction by combining bone morphogenetic protein (BMP)-2 with a bioactive novel nanocomposite, *Bone Joint Res.*, 2012; 1: 145-151.
- Thibault M., Astolfi M., KhanhN., LavertuM., DarrasV., MerzoukiA., BuschmannM.D., Excess polycation mediates efficient chitosan-based gene transfer by promoting lysosomal release of the polyplexes, *Biomaterials.*, 2011 ; 32: 4639-4646.
- Transferrin-Binding Proteins—Advances in Research and Application: Ed 2012, ScholarlyBrief, Edited by Acton Q. A, ScholarlyEditions™.
- Tsao S. W., Mok S.C., Fey E.G., Fletcher J.A., Wan T.S.K., Chew E. C., Muto M.G., Knapp R.C., Berkowitz R.S., Characterization of human ovarian epithelial cells immortalized by human papilloma viral oncogenes (HPV E6/E7 ORFs). *Exp. Cell Res.*, 1995; 218: 499-507.
- Vallier L., Rugg-Gunn P.J., Bouhon I.A., Andersson F.K., Sadler A.J., Pedersen R.A., Enhancing and diminishing gene function in human embryonic stem cells, *Stem Cells.*, 2004; 22: 2–11.

- Vogelstein B., Kinzler K.W., p53 function and dysfunction Cell., 1992; 70:523-6.
- Walker S., Sofia M.J., Kakarla R., Kogan N.A., Wierichs L., Longley C.B., Bruker K., Axelrod H.R., Midha S., Babu S., Kahne D., Cationic facial amphiphiles: A promising class of transfection agents, Proc Natl Acad Sci, USA. 1996; 93:1585-1590.
- Wang D., Li L., Zhang P., Synthesis of some neutral, water-soluble carbodiimides and their use in the formation of peptide bonds, Sci. Sin. Ser. B., 1987; 30: 449-459.
- Wang Xu-Li, Jensen Randy, Lu Zheng-Rong., A novel environment-sensitive biodegradable polydisulfide with protonatable pendants for nucleic acid delivery, J. of Controlled Release., 2007; 120: 250-258.
- Xu G., Wen X., Hong Y., Du H., Zhang X., Song J., Yin Y., Huang H., Shen G., An anti-transferrin receptor antibody enhanced the growth inhibitory effects of chemotherapeutic drugs on human glioma cells, Int Immunopharmacol., 2011 ;11:1844-9.
- Xue W., Zender L., Miething C., Dickins R.A., Hernando E., Krizhanovsky V., Lowe S. W., Senescence and tumour clearance is triggered by p53 restoration in murine liver carcinomas, Nature, 2007; 445: 656-660.
- Yang F., Moss L.G., Phillips G.N Jr., The molecular structure of green fluorescent protein, *Nat Biotechnol.*, 1996;14:1246–51.
- Zhang J.W. and Zhu X.X., Biomaterials made of bile acids, Science in China Series B: Chemistry, 2009; 52: 849-861
- Zheng M., Zhong Y., Meng F., Peng R., Zhong Z., Lipoic acid modified low molecularweight polyethylenimine mediates nontoxic and highly potent in vitrogene transfection, Mol Pharm., 2012; 8: 2434-43.